EP_4 Antagonist-Elicited Extracellular Vesicles from Mesenchymal Stem Cells Rescue Cognition/Learning Deficiencies by Restoring Brain Cellular Functions

Shih-Yin Chen,[a] Meng-Chieh Lin,[a] Jia-Shiuan Tsai,[a] Pei-Lin He,[a] Wen-Ting Luo,[a] Harvey Herschman,[b,c,d] Hua-Jung Li [a]

Key Words. PGE_2/EP_4 signaling • Mesenchymal stem cell • Extracellular vesicle • Exosome • Cognition and memory • Astrocyte • Inflammation

aInstitute of Cellular and System Medicine, National Health Research Institutes, Miaoli, Taiwan, Republic of China; bDepartment of Molecular & Medical Pharmacology, University of California, Los Angeles, Los Angeles, California, USA; cDepartment of Biological Chemistry, University of California, Los Angeles, Los Angeles, California, USA; dMolecular Biology Institute, University of California, Los Angeles, Los Angeles, California, USA

Correspondence: Hua-Jung Li, Ph.D., R2-5031, 35 Keyan Road, Zhunan, Miaoli County 35053, Taiwan, Republic of China. Telephone: 886037246166, ext. 38306; e-mail: annli@nhri.org.tw

Abstract

Adult brains have limited regenerative capacity. Consequently, both brain damage and neurodegenerative diseases often cause functional impairment for patients. Mesenchymal stem cells (MSCs), one type of adult stem cells, can be isolated from various adult tissues. MSCs have been used in clinical trials to treat human diseases and the therapeutic potentials of the MSC-derived secretome and extracellular vesicles (EVs) have been under investigation. We found that blocking the prostaglandin E_2/prostaglandin E_2 receptor 4 (PGE_2/EP_4) signaling pathway in MSCs with EP_4 antagonists increased EV release and promoted the sorting of specific proteins, including anti-inflammatory cytokines and factors that modify astrocyte function, blood–brain barrier integrity, and microglial migration into the damaged hippocampus, into the EVs. Systemic administration of EP_4 antagonist-elicited MSC EVs repaired deficiencies of cognition, learning and memory, inhibited reactive astrogliosis, attenuated extensive inflammation, reduced microglial infiltration into the damaged hippocampus, and increased blood–brain barrier integrity when administered to mice following hippocampal damage. STEM CELLS TRANSLATIONAL MEDICINE 2019;8:707–723

Significance Statement

Hippocampal damage occurring with many central nervous system (CNS) diseases and traumatic brain injury is responsible for cognition, learning, and memory impairments. However, CNS regenerative capacity is extremely limited. This study demonstrates that blocking PGE_2/EP_4 signaling induces extracellular vesicles (EVs) from mesenchymal stem cells (MSCs) and that these EP_4-antagonist elicited MSC EVs carry cargo responsible for MSC properties. This study suggests that EP_4 antagonist-elicited MSC EVs may replace MSCs in therapy for CNS disease because both of their increased therapeutic efficacy and of reduced adverse effects such as complications of implantation, ectopic tissue formation, and unwanted engraftment. More generally, the data suggest that EP_4 antagonist-elicited MSC EVs may be useful for therapies of a variety of pathologies.

Introduction

Damage and/or degeneration of the hippocampus frequently result in impairment of memory and other intellectual functions [1–3]. The self-regenerative capacity of the CNS is extremely limited. Recently, therapeutic effects of mesenchymal stem cells (MSCs) for neurological diseases such as cerebral infarction, Alzheimer's disease (AD), and Parkinson's disease (PD), have been reported [4–7]. MSCs reside in many tissues and body fluids, for example, circulating blood, cord blood, bone marrow, amniotic fluid, placenta, adipose tissues, and dental pulp [8]. Since MSCs are available from adults and can be easily isolated, MSCs are excellent sources of autologous stem cells; these cells can be isolated either from patients themselves or from their predeposited tissues/fluid. The multipotency and easy accessibility of MSCs make them a promising tool for stem cell therapy. However, less than 1% of implanted MSCs are capable of engrafting and only a small percentage of those engrafted MSCs differentiate into functional replacement tissue in damaged areas [9, 10]. Preclinical studies suggest that the therapeutic effects of MSC transplantation do not result from the permanently engrafted cells. Instead, dynamic paracrine interactions between MSCs and damaged tissues

appear to contribute to MSC therapeutic activity [11]. These findings suggest that therapeutic effects of MSCs, including their effects on CNS, rely mainly on extracellular components.

Extracellular vesicles (EVs) can act as agents to exert physiological actions through cell–cell communication [12]. MSC-derived EVs have emerged recently as an application for regenerative medicine; systemic EV administration, including allogeneic MSC-derived EVs, has not triggered adverse effects [13]. However, MSC-derived EV therapy is still a developing research area that needs to be optimized to improve their regenerative potential. Here, we describe MSC culture conditions that can trigger release of EVs with increased regenerative potential.

We previously showed that prostaglandin E$_2$/prostaglandin E$_2$ receptor 4 (PGE$_2$/EP$_4$) signaling is essential to maintain stemness both of mammary epithelial stem cells (MaSCs) [14] and of mammary cancer stem cells (CSCs) [15]. Blocking PGE$_2$/EP$_4$ signaling of MaSCs elicits EV release from MaSCs and promotes sorting of the factors essential for MaSC properties into their EVs. EP$_4$ antagonist-elicited EVs from MaSCs which carry MaSC properties can induce mammary gland formation in mice [14]. Similarly, blocking PGE$_2$/EP$_4$ signaling of mammary cancer CSCs elicits EV release from the CSCs and promotes sorting of the factors essential for their CSC properties into the EVs [15]. Moreover, EVs from EP$_4$ antagonist treated CSCs can convert mammary cancer epithelial cells to CSCs [15], just as EP$_4$ antagonist elicited EVs from MaSCs can convert mammary epithelial cells to stem cells capable of eliciting mammary gland formation [14].

PGE$_2$ signaling is also essential for MSC homeostasis [16–18]. Here, we demonstrate that EP$_4$ antagonism induces EVs from MSCs and that these EP$_4$ antagonist-induced MSC EVs, which carry cargo responsible for many MSC properties, can be used in place of MSCs for stem cell therapy. We demonstrate that EP$_4$ antagonist-elicited MSC EVs have therapeutic effects on hippocampal damage. EP$_4$ antagonist-elicited MSC EVs can rescue hippocampal CA1 damage-mediated cognition and learning deficiencies and modulate astrogliosis, microglial infiltration into the wounded hippocampus, inflammatory responses, and blood–brain barrier (BBB) properties. These findings suggest leveraging MSC regenerative medicine of CNS damage and disease in a more effective way.

MATERIALS AND METHODS

Cell Culture

The different batches of human bone marrow MSCs (passage 1) were obtained from Sciencells (Carlsbad, CA). The MSCs were derived from 21-week-old male donors. MSCs were propagated in low glucose Dulbecco's modified Eagle's medium containing 5% fetal bovine serum (FBS) with penicillin–streptomycin. FBS contains bovine-derived EVs. The bovine derived EVs were removed by ultracentrifugation before the FBS was used for MSC culture [19]. MSC were passaged for not more than eight passages. See Supporting Information Materials and Methods for information concerning primary hippocampal neural cells.

EV Isolation

EVs were isolated from MSC culture media by differential ultracentrifugation as previously described [14]. Briefly, MSCs were treated with dimethyl sulfoxide (DMSO) vehicle or 20 μg/ml EP$_4$ antagonist GW627368X (GW) for 4 or 8 days, as indicated in the figure legends. Culture media were collected

and were replaced with fresh media supplemented with DMSO or GW every 4 days. The collected culture media were centrifuged at 300g for 5 minutes to remove cells (P1), at 2,000 g for 20 minutes (P2), then at 10,000 g for 30 minutes (P3) all at 4°C. Finally, EVs (P4) were separated from the supernatant by centrifugation at 110,000g for 60 minutes. The EV pellet was washed once in phosphate-buffered saline (PBS) and then resuspended in PBS for further analysis and injection.

Animal Experiments

All research involving animals complied with protocols approved by the NHRI Committee on Animal Care. B6.CBA-Tg(Camk2a-tTA) and B6.Cg-Tg(tetO-diphtheria toxin A [DTA]) mice were obtained from Jackson Lab. Doxycycline (Dox) was removed from the diet of 6-week-old tetO-DTA mice and Camk2a-tTA/tetO-DTA mice for 25 days. On the 26th day, doxycycline (2,000 ppm) was returned to the mouse chow. Mice were maintained on tetracycline-enriched chow, except for the 25-day Dox-free period for brain lesion. After the Dox-free period, mice were injected with 100 μl PBS or EVs derived from MSCs or EP$_4$ antagonist-elicited MSCs (15 μg EV/injection, twice) via intracardiac injection as indicated in the figure legends. After the injection, mice were subjected for behavioral analysis (e.g., novel object recognition test [NORT], novel location recognition test [NLRT], Morris water maze [MWM]) at the time points indicated in the figure legends. Mice were sacrificed at the time points indicated in the figure legends and the brains were collected for further analysis (e.g., exon arrays, immunohistochemistry, Western blotting).

Tissue Preparation and Immunofluorescence from Tissue Sections

Paraformaldehyde-fixed tissues were embedded in paraffin blocks and cut into 4-μm sections. Hematoxylin and eosin staining was conducted according to conventional procedures. Tissue sections were deparaffinized/hydrated and were then subjected to antigen retrieval in citrate buffer (pH 6.0) for 10 minutes. The sections were incubated with primary antibodies overnight at 4°C and then with secondary antibodies for 1 hour at room temperature. Cell nuclei were visualized with DAPI. Slides were mounted with ProLong Gold Antifade Reagent and imaged using a TCS SP5 II confocal microscope. The following antibodies were used: anti-NeuN (Millipore, [Burlington, MA], ABN78), anti-complement 3 (Abcam, [Cambridge, U.K.], ab200999), anti-COX-2 (Thermo Fisher Scientific, MA), anti-GFAP (Millipore, Mab360), anti-S100β (Abcam, ab52642), anti-Iba1 (Abcam, ab5076), anti-β3 tubulin (Abcam, ab5076), and anti-CLDN5 (Thermo Fisher, 34-1600). Signal quantification was performed using ImageJ software. Immunohistochemistry quantification was performed using ImageJ, following the ImageJ User Guide. For quantitation of glial fibrillary acidic protein (GFAP)-positive cells, S100B-positive cells, and Iba1-positive cells, 8-bit images of the hippocampus CA1 region were loaded into ImageJ. The signal-positive area was calculated using "Analyze Particles" under the ImageJ "Analyze" function. For quantitation of CLDN5 signal, 8-bit images of the hippocampus CA1 region were loaded into ImageJ. The signal intensity was measured using "Measure" under the ImageJ "Analyze" function. The CLDN 5 intensity was normalized by the area of the BBB structure, which was defined by the area of GFAP-positive astrocyte endfeet.

Statistical Analysis

Prism 7 was used for data presentation and statistical analysis. For Figures 1B, 1G, 1H, 1J, 1K, 2B–2D, 2G, 3C, 3E, 3F, 3G, 5E,

6A, 6B, 6E, Student's *t* test was used. The level of significance was set at $p \leq .05$. See figure legends for more information.

See Supporting Information Materials and Methods for more information regarding additional experimental methods.

RESULTS

EP$_4$ Receptor Antagonism Modulates the Phenotypes of MSCs and Decreases Their Differentiation Potential

To investigate whether EP$_4$ signaling is necessary to maintain MSC properties, we treated human bone marrow MSCs with the EP$_4$ antagonist GW and assessed the stem cell traits of the control and pharmacologically treated cells. GW treatment induced an epithelial morphology in MSCs within 48 hours (Fig. 1A). The GW-treated MSCs formed cobblestone-like, epithelial islands in the presence of GW. In contrast, MSCs cultured in the absence of GW maintained their preexisting mesenchymal morphology. Although GW treatment slightly decreased the numbers of MSCs (Fig. 1B), it did not cause significant cell death, measured by the apoptotic sub-G1 fraction (Fig. 1C) and by the activation of the executioner of apoptosis, caspase 3 (Fig. 1D).

GW treatment decreased the level of the MSC surface markers CD90 and CD105 (Fig. 1E). MSCs can be identified based on their expression of surface markers, including CD90 and CD105. The expression of CD90 and CD105 MSC surface markers reflects MSC potentials to differentiate into osteocytes and adipocytes [20, 21]. Therefore, decreases of CD90 and CD105 suggest decreases of the stem cell capacity of MSCs. Since we observed that EP$_4$ antagonist GW decreased MSC surface CD90 and CD105, we investigated whether EP$_4$ antagonism modulated the differentiation potential of MSCs. MSCs pretreated with vehicle or EP$_4$ antagonist GW were subjected to either osteogenic or adipogenic differentiation. The EP$_4$ antagonist treatment was suspended during the subsequent differentiation processes. Compared with the vehicle-pretreated MSCs, the GW-pretreated MSCs formed 89% fewer osteocytes in the osteogenic condition (Fig. 1F, 1G). The expression of the osteogenesis makers runt-related transcription factor 2 (RUNX2) and alkaline phosphatase (ALP) [22] was attenuated in the GW-pretreated MSCs in the osteogenic condition, compared with that of the vehicle-pretreated MSCs (Fig. 1H). Similarly, the GW-pretreated MSCs formed 70% fewer adipocytes when compared with the vehicle-treated MSCs (Fig. 1I, 1J) and the expression of the adipogenesis makers lipoprotein lipase (LPL) and peroxisome proliferator-activated receptor γ (PPARγ) [22], was suppressed in the GW-pretreated MSCs in the adipogenic condition (Fig. 1K). These data demonstrate that EP$_4$ antagonism decreases the differentiation potential of MSCs.

EP$_4$ Antagonism Elicits MSCs Release of EVs

In addition to causing MSCs to lose stem cell properties (mesenchymal morphology, stem cell markers, and differentiation potential), EP$_4$ antagonism induced EV release from MSCs. The conditioned media of MSCs treated with vehicle or with the GW EP$_4$ antagonist for 4 days were collected and subjected to differential centrifugation for EV isolation. Nanoparticle tracking analysis showed that both vehicle-treated and GW-treated MSCs released abundant ~100 nm membrane vesicles (Fig. 2A). The size of the vesicles corresponded with that of exosomes; 50–150 nm [23]. Compared with vehicle DMSO, the EP$_4$ antagonist elicited a twofold increase in EVs released from MSCs (Fig. 2B). The amounts of total protein

in vehicle-induced and GW-induced EVs corresponded to the numbers of the EVs (Fig. 2C, 2D). Consequently, in our subsequent experiments, we used the amounts of total EV protein to compare the relative numbers of EVs.

Large amounts of general exosome markers (e.g., CD63 and TSG101 [23, 24]) were present in the EVs released by GW-EP$_4$ antagonist treated MSCs (Fig. 2E). In contrast, little or no exosome marker proteins were detected in the EV fraction of vehicle-treated MSCs (Fig. 2E). These data suggest that the EP$_4$ antagonist-elicited MSC EVs were enriched in exosomes. The EVs of GW-treated MSCs were enriched in proteins essential to maintain mesenchymal/stem-like properties (Fig. 2E). Compared with vehicle-treated MSCs, larger amounts of proteins contributing to mesenchymal cell morphology (e.g., N-cadherin [N-cad], twist), MSC markers (e.g., CD105, CD90, CD44), and stem cell homeostasis (e.g., β-catenin [25, 26], twist [27, 28]) were released from the GW-treated MSCs via EVs (Fig. 2E). These data demonstrate that EP$_4$ signaling regulates MSC EV release both in quantity and in composition; EP$_4$ antagonism promotes MSCs to release, via EVs, proteins required to maintain MSC properties. We suggest that these EP$_4$ antagonist-elicited, EV-mediated losses contribute to the changes in morphology, stem cell identity, and differentiation potential of GW-treated MSCs (Fig. 1).

EP$_4$ Antagonist-Elicited MSC EVs Contain Anti-Inflammatory Cytokines and Neuron-Supporting Proteins

MSCs are potent immunomodulators and often affect immune responses by released cytokines (e.g., interleukin [IL]-10 and TGFβ) [29]. The vehicle-induced EVs and GW-induced MSC EVs (GWEVs) were subjected to cytokine analyses, using cytokine arrays (Fig. 2F, 174 cytokines analyzed). Among the analyzed cytokines, elevated levels of 11 cytokines, including brain-derived neurotrophic factor (BDNF), RANTES, TIMP1, LIF, BMP-7, IL-18Rβ, and DR6, are detected in the GWEVs (Fig. 2F and Supporting Information Fig. S1). The increases of specific cytokines and proteins (e.g., IL-2, IL-10, RANTES, vascular endothelial growth factor [VEGF]-a, BDNF) in GWEVs from different batches of MSCs was confirmed by quantitative Bio-Plex cytokine assays (Fig. 2G) and Western blotting (Fig. 2H). The results suggest that GWEVs are enriched in IL-2 anti-inflammatory cytokine [30], IL-10 anti-inflammatory cytokine [30], VEGF-a/LIF/BMP7 neurogenesis promoting factors [31–33], TIMP-1 BBB integrity-supporting factors [34, 35], BDNF neuron-promoting/anti-inflammatory/astrocyte-modulating cytokine [36–39], RANTES neuroprotective mediator [40, 41], and N-cad/BMP7 neuritogenesis-promoting factors [42]. The enriched EV cargos suggest that EP$_4$ antagonist-elicited EVs may have the potential to reduce inflammation and to repair brain damage and/or degeneration.

EP$_4$ Antagonist-Elicited MSC EVs Rescue Memory and Learning Deficiencies Caused by Hippocampus Damage

Because the hippocampal CA1 region plays a critical role in cognition, learning, and spatial/contextual memory [43, 44], it is an essential target for the treatment of dementia and disability caused by brain damage. Prior reports suggest that MSC implantation [45] and factors released by MSCs [46] can modulate brain damage. Our previous studies suggest that EP$_4$ antagonism of MaSCs elicits EVs whose cargo can modulate the phenotype of mammary epithelial cells [14], and that EP$_4$ antagonism of mammary tumor CSCs elicits EVs whose cargo can modulate the phenotype of mammary cancer epithelial
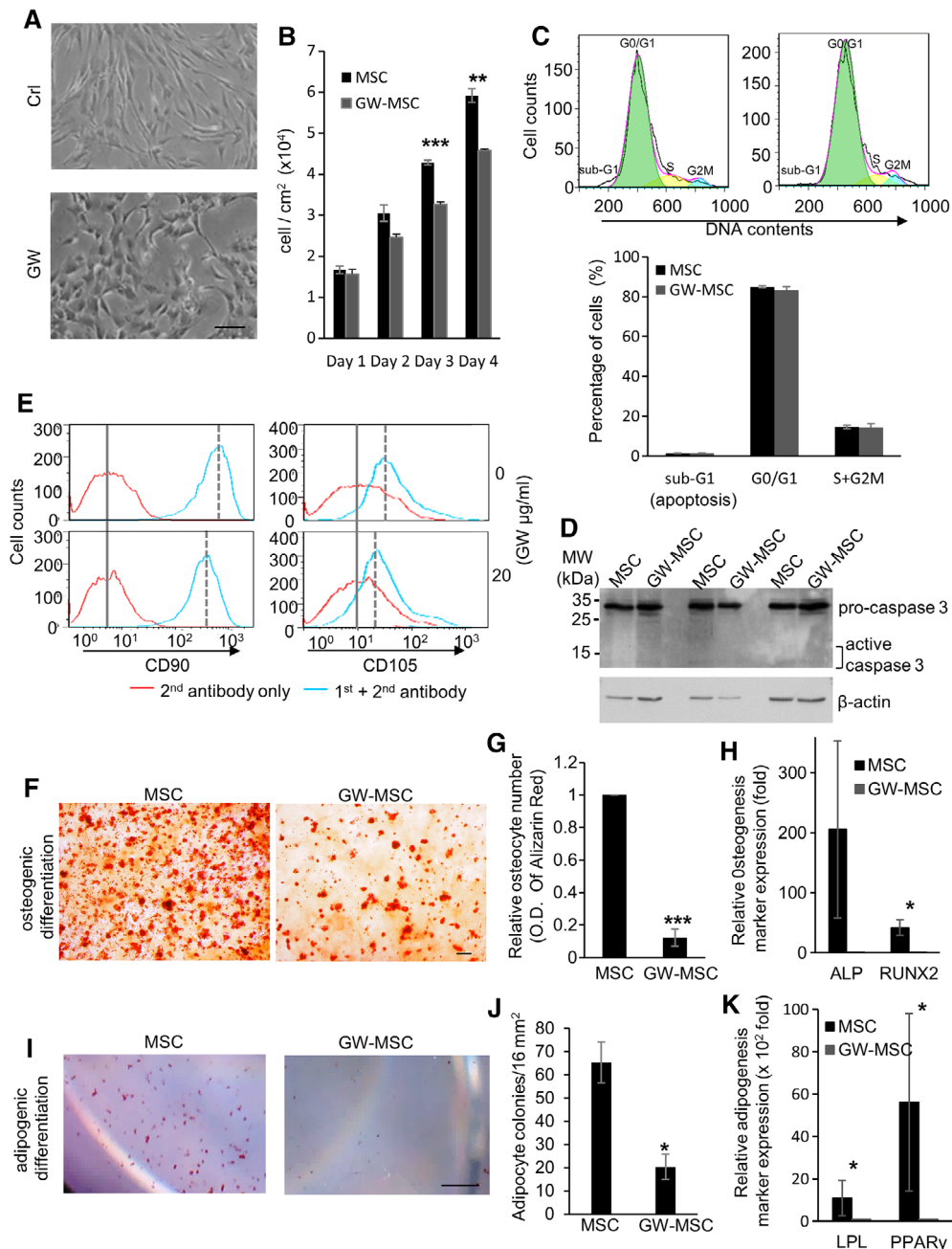
Figure 1. Blocking prostaglandin E$_2$/prostaglandin E$_2$ receptor 4 signaling of mesenchymal stem cells decreases the stem cell properties. **(A):** Bright-field images of mesenchymal stem cells (MSCs) treated with DMSO vehicle (Crl) or GW627368X (GW; 20 μg/ml) for 96 hours. Scale bar: 100 μm. **(B):** The numbers of MSCs treated with DMSO (MSC) or GW (GW-MSC) for 4 days. Data are mean ± SEM (n = 3). **, $p \le .01$; ***, $p \le .001$. **(C):** Sub-G1 profiles of MSCs treated with vehicle (MSC, upper left panel) or GW (GW-MSC, upper right panel) for 96 hours, using flow cytometry. DNA fragmentation in apoptotic cells is revealed by sub-G1 population on DNA content. Percentages of sub-G1, G0/G1, and S + G2M cell populations are calculated using FlowJo (bottom panel). Data are mean ± SEM (n = 3). **(D):** Activation of apoptotic protein caspase 3 upon proteolytic cleavage in MSCs treated with vehicle (MSC) or GW (GW-MSC), measured with Western blotting. **(E):** Cell surface CD90 and CD105 of MSCs treated with vehicle (upper panels) or GW (lower panels) for 4 days. **(F–H):** Osteogenic differentiation potential of MSCs and GW-pretreated (4 days) MSCs (GW-MSCs). The MSCs and GW-MSCs were induced to differentiate into osteocytes and the levels of osteocytes were measured by Alizarin Red S staining. Scale bar: 100 μm. The levels of Alizarin Red in the derived osteocytes were measured by O. D. 405 nm and were plotted in panel (G). The mRNA levels of osteogenesis makers were measured by qPCR and plotted in panel (H). Data are mean ± SEM (n = 3). *, $p \le .05$; ***, $p \le .001$. **(I–K):** Adipogenic differentiation potential of MSCs and GW-MSCs. The MSCs and GW-MSCs were induced to differentiate into adipocytes and the levels of adipocytes were measured by Oil Red O staining. Scale bar: 1 mm. Quantification of adipocyte colonies per 16 mm^2 is in panel (J). The mRNA levels of adipogenesis makers were measured by qPCR and plotted in panel (K). Data are mean ± SEM (n = 3). *, $p \le .05$.

cells [15]. These observations led us to examine the consequences of treating mice with damaged hippocampi with the EP$_4$ antagonist-induced EVs from MSCs.

To examine whether the EP$_4$ antagonist-elicited MSC EVs have therapeutic potential for hippocampal neuron damage, we used a mouse model carrying transgenes for inducible
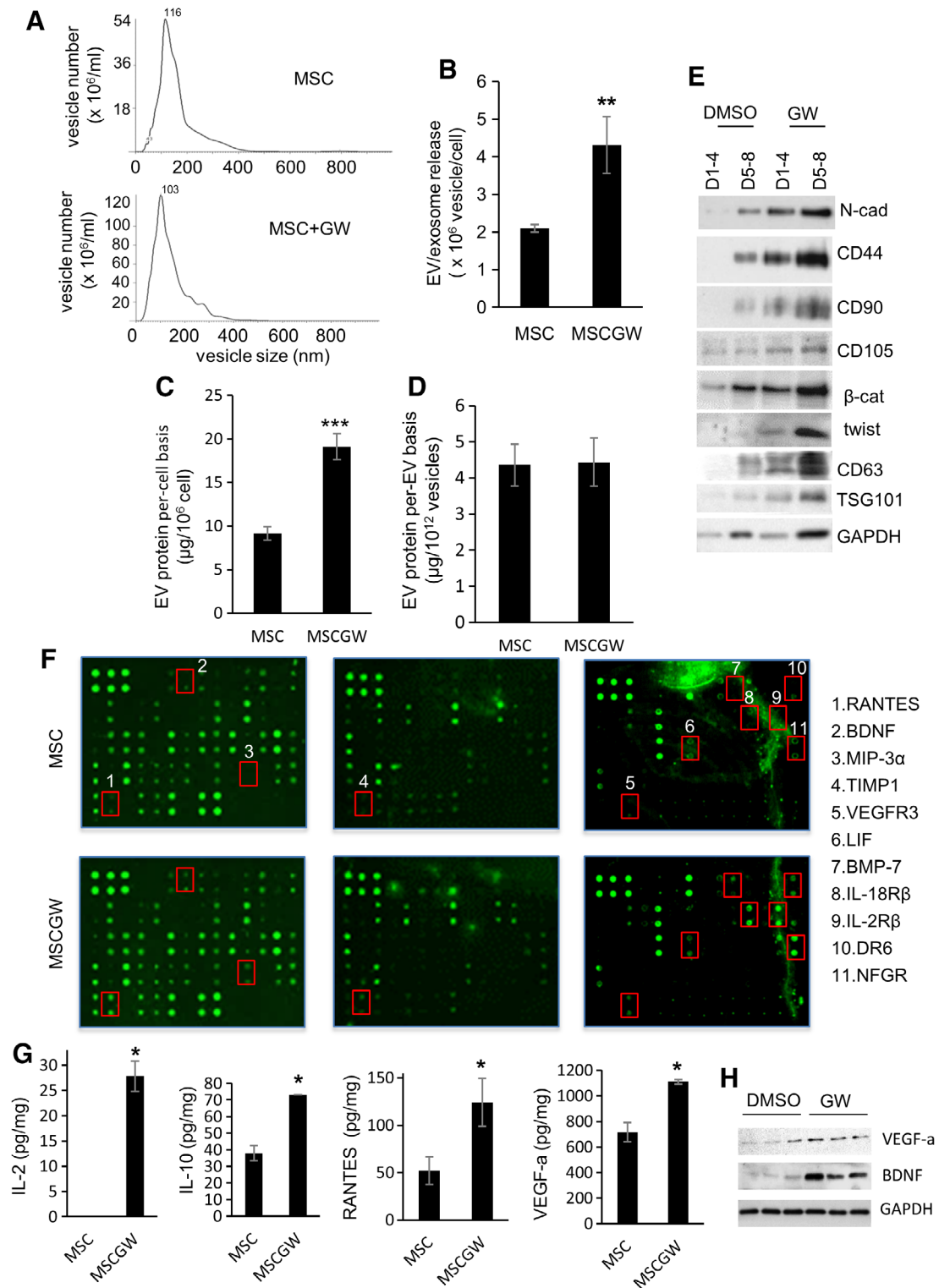
Figure 2. Blocking prostaglandin E_2/prostaglandin E_2 receptor 4 signaling of mesenchymal stem cells (MSCs) elicits the release of extracellular vesicles (EVs) and exosomal protein sorting. **(A, B):** Vesicle size and numbers of EVs released from MSCs and GW627368X (GW)-treated MSCs (MSC-GW). Nanoparticle tracking analysis determined the vesicle size in panel (A), vesicle numbers are in panel (B). Data are mean ± SEM (n = 3). **, p ≤ .005. **(C, D):** Total EV proteins released from MSCs and MSCGWs were measured, on a per-cell basis (C) and on a per-EV basis (D). Data are mean ± SEM (n = 3). ***, p ≤ .001. **(E):** Proteins were analyzed in the EVs from the same number of MSCs. The EVs were isolated from the same number of DMSO-treated or GW-treated MSCs, and compared on a per-cell basis. D1–4 are proteins in EVs isolated from day 1 to 4 cell cultures. D5–8 are EVs isolated from day 5 to 8 cell cultures. **(F, G):** Cytokines were measured in the same number of EVs from MSCs or GW-treated MSCs (MSCGW), compared on a per-vesicle basis. Cytokines were measured using cytokine arrays in panel (F) and bio-Plex pro cytokine assays in panel (G). The cytokines differentially expressed in the EVs are listed in panel (F). Data are mean ± SEM (n = 3). *, p ≤ .05. (C): Proteins from the same number of EVs from different batches of MSCs (DMSO) and GW-treated MSCs (GW) were analyzed.

hippocampal CA1 neuron damage. Since human MSCs are not immunologically reactive and can be tolerated by mice [47], we can explore therapeutic potentials of human MSC-derived EVs in this mouse preclinical model. Camk2a-tTA/tetO-DTA transgenic mice express the tetracycline/doxycycline-suppressed transactivator protein (tTA) under control of the hippocampal CA1-specific calcium-calmodulin-dependent kinase II (Camk2a) promoter and DTA under the control of a tetracycline/doxycycline-responsive element (Fig. 3A). Under doxycycline (Dox) treatment, DTA expression is suppressed in the transgenic mice. Once Dox is withdrawn, DTA specifically expressed in the neurons of the hippocampus CA1 region causes damage. In the hippocampus, the CA1 region contains a unique, compact layer of pyramidal neurons consisting of ~8 rows of neuron bodies [48]. This region has extensive axon neurites protruding out from the pyramidal neuron layer. The number of hippocampal CA1 pyramidal neurons is positively correlated with the thickness of the CA1 pyramidal cell body layer [49]. A 25-day Dox withdrawal starting from the age of 6 weeks caused decreases of the thickness of neuron layers in hippocampus CA1 of Camk2a/DTA mice (Fig. 3B, right panels, damaged control). The induced hippocampal damage decreased this neuron layer in hippocampi CA1 of Camk2a/DTA mice. Compared with the control tetO-DTA mice (DTA) which did not carry the tTA transgene (undamaged control [UC]), the numbers of NeuN-positive neurons (a marker for neurons [50]) in hippocampus CA1 were greatly decreased in the Camk2a/DTA mice after the 25-day Dox withdrawal (Fig. 3B, bottom panels), demonstrating neuronal damage.

Since the hippocampus plays important roles in memory consolidation and in spatial memory for navigation [51], we examined whether the EP₄ antagonist-elicited MSC GWEVs can rescue memory deficiencies of the Camk2a/DTA mice caused by hippocampal damage. The EVs were labeled with PKH26 dye after purification. To analyze EV uptake in hippocampus CA1, PKH26-labeled MSC EVs and GWEVs were administrated via intracardiac injection. MSC EVs and MSC GWEVs were delivered in equal amounts into the hippocampal CA1 region (Fig. 3C and Supporting Information Fig. S2). Consequently, in our subsequent experiments, MSC EVs, GWEVs, and PBS were given to the mice via intracardiac injection.

A 25-day Dox withdrawal was performed, starting from the age of 6 weeks, for DTA mice and Camk2a/DTA mice (Fig. 3D). After Dox withdrawal, the mice received two rounds of PBS, MSC EV, or MSC GWEV injections, at the time points indicated by the green arrows in Figure 3D. Since repeated administration of MSCs does not induce immunoreactivity [52–56], the lack of MSC immunogenicity allowed us to optimize the therapeutic effects of MSC EVs and GWEVs by using two sequential injections [57]. At 20 days after the last injection, mice were subjected to behavior tests (e.g., NLRT, NORT, and MWM navigation test) to evaluate memory consolidation and spatial memory for the four groups of mice (Fig. 3D).

NLRT and NORT have been widely used in evaluating rodent memory formation [58]. Due to the natural preference for novelty displayed by rodents, mice with functional hippocampi spend more time exploring the object at a novel location (Fig. 3E) and exploring the novel object (Fig. 3F) than do mice with hippocampal damage. Although the undamaged DTA mice spent nearly 70% of the test time exploring the novel objects in both NLRT and NORT, PBS-injected Camk2a/DTA mice spent almost equal time (i.e., not showing any preference) in both tests, on the original object and the novel object (Fig. 3E, 3F). These results demonstrate that the

Cam2a/DTA mice with hippocampal damage cannot distinguish the original and novel objects in both NLRT and NORT. These analyses suggest the hippocampal damage in camk2a/DTA mice caused memory deficiencies.

Like PBS-injected Camk2a/DTA mice, MSC EV-injected Camk2a/DTA mice did not spend more time exploring the novel objects in either NLRT (Fig. 3E) or NORT (Fig. 3F); systemic MSC EV administration did not improve the cognition and memory deficiencies of hippocampal-damaged Camk2a/DTA mice. In contrast, MSC GWEV-injected Camk2a/DTA mice, like control mice with no hippocampal damage, also spent nearly 70% of their test time exploring the novel objects in both NLRT (Fig. 3E) and NORT (Fig. 3F). Systemic EP₄ antagonist-elicited MSC EV administration resulted in significant recovery of the preference of camk2a/DTA mice to explore the novel objects, reaching levels that were statistically indistinguishable to the preferential exploratory levels of control DTA mice in both NLRT (Fig. 3E) and NORT (Fig. 3F). These results suggest that EP₄ antagonist-elicited MSC EVs rescue the memory deficiencies caused by hippocampal CA1 damage.

The Morris water maze (MWM) test is a measure of hippocampal-dependent spatial navigation and reference memory [59]. In the MWM test, the mice refer to position cues around the pool to navigate from a start location in a swimming pool to a submerged platform. The mice, relying on their spatial memory, should be able to decrease the time to find the platform in navigation during the 5-day trial. In the test, the DTA UC mice significantly decreased the time required to find the platform each day of the repeated 5-day testing period (Fig. 3G, black line). In contrast, the time to find the platform for the PBS-injected Camk2a/DTA mice did not decrease during the 5-day trial (Fig. 3G, green line), suggesting that control Camk2a/DTA mice lost the spatial memory ability that would help them to locate the platform in the MWM navigation test. Like PBS-injected Camk2a/DTA mice, the time to find the platform for MSC EV-injected Camk2a/DTA mice did not significantly decrease during the 5-day trial (Fig. 3G, red line). Both PBS-injected and MSC EV-injected Camk2a/DTA mice performed similarly in the MWM navigation test; systemic administration of MSC EVs did not rescue the spatial memory deficiency caused by the hippocampal damage. In contrast, the MSC GWEV-injected Camk2a/DTA mice spent significantly less time finding the platform on both day 4 and day 5 of the analysis (Fig. 3G, blue line); indeed, MSC GWEV-injected mice performed as well as DTA mice in platform identification on days 4 and 5 of the trial. These results demonstrate that EP₄ antagonist-elicited MSC GWEVs rescue the spatial memory deficiency caused by the hippocampal damage.

EP₄ Antagonist-Elicited MSC EVs Increase the Expression of Genes Involved in Astrocyte Differentiation, BBB Integrity, and Anti-Inflammation

To analyze the molecular consequences of EP₄ antagonist-elicited MSC EVs (GWEVs) on hippocampal damage of Camk2a/DTA mice, we compared gene expression in the hippocampi of PBS-treated, MSC EV-treated, and MSC GWEV-treated Camk2a/DTA mice with hippocampal damage. We anticipated that this study would define critical biochemical and cellular functions that might be altered in the damaged hippocampus and require modulation by MSC GWEVs cargo to restore functional recovery. As indicated in Figure 4A, two rounds of PBS or EV injections were given to each Camk2a/DTA mouse after the 25-day Dox withdrawal. Five days after the last injection, mouse
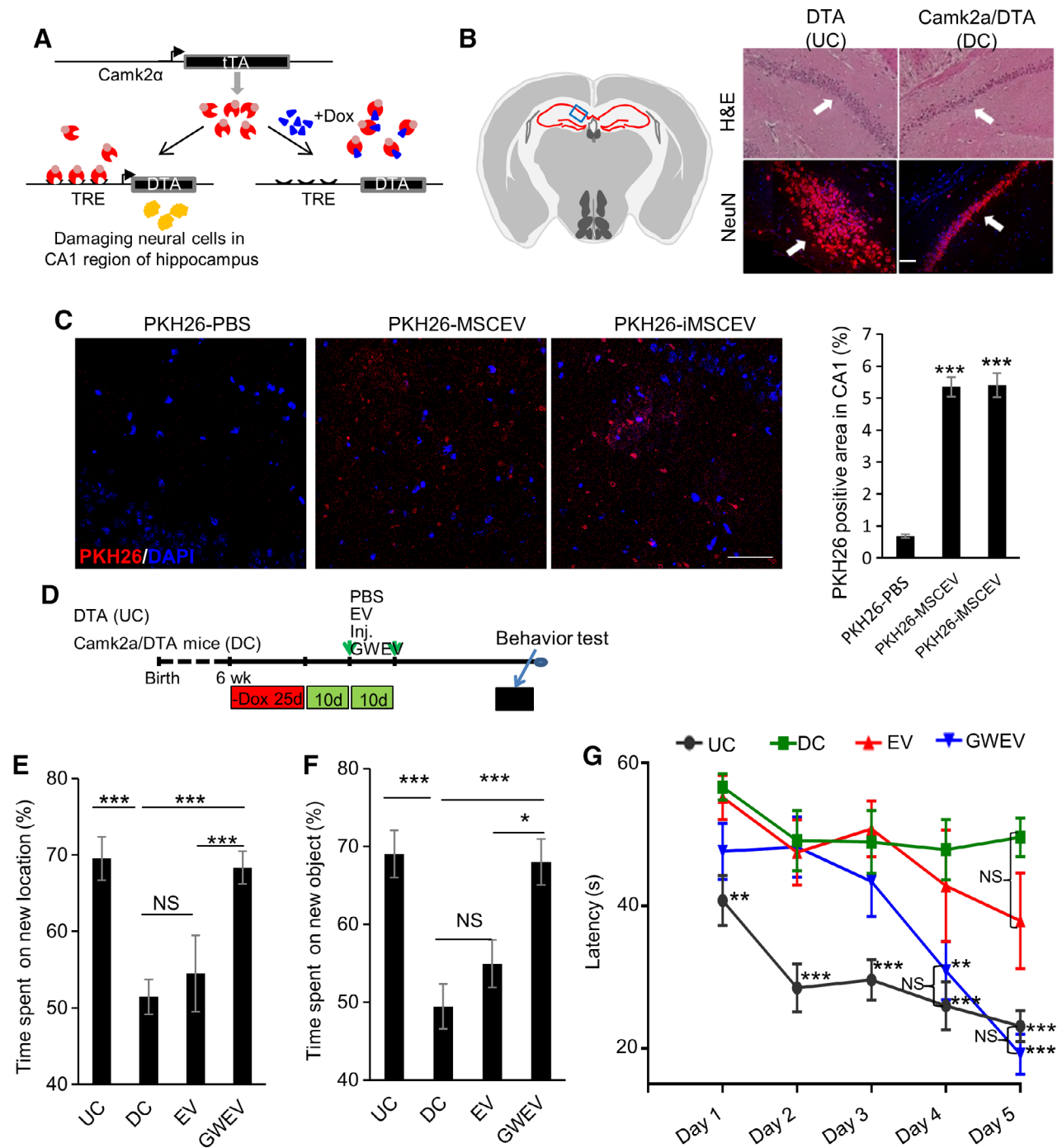
Figure 3. Prostaglandin E_2 receptor 4 antagonist-elicited mesenchymal stem cell (MSC) extracellular vesicles (EVs) rescue memory and learning deficiencies caused by hippocampal damage. **(A):** The tetracycline/doxycycline-regulated gene switch of Camk2a-tTA/tetO-diphtheria toxin A (DTA) transgenic mice. Camk2a-tTA/tetO-DTA transgenic mice express the tetracycline/doxycycline-suppressed transactivator protein (tTA) under control of the Camk2a promoter. DTA is not expressed in the presence of Dox, but is expressed in the absence of Dox, causing damage in hippocampus CA1. **(B):** Hematoxylin and eosin staining and anti-NeuN immunofluorescence in the hippocampus of Dox-withdrawn tetO-DTA mice (DTA, undamaged control [UC]) and Camk2a-tTA/tetO-DTA (Camk2a/DTA, damaged control [DC]) mice. Arrows: hippocampus CA1 neurons. Scale bar: 100 μm. Left panel: the blue box in schematic depiction of the brain section represents the anatomic region analyzed by staining. Red lines, hippocampus. **(C):** EV uptake into hippocampus CA1. PKH26-labeled MSC EVs, PKH26-labeled GW-induced MSC EVs (GWEVs), and negative control (see Supporting Information Materials and Methods) were administrated into mice via intracardiac injection. At 16 hours after the injection, mice were sacrificed and the brains were collected for further analysis. Cell nuclei were stained with DAPI (blue). Quantification of PKH26-positive area in hippocampus CA1 of the mice described in the right panel. Data are mean ± SEM (n = 9 for each group). ***, $p \leq .001$. Scale bar: 50 μm. **(D):** The scheme of the mice learning and memory experiments, indicating the time points of damage induction, EV administration, and behavioral analyses. **(E–G):** The time spent by Dox-withdrawn DTA mice (UC) and by Dox-withdrawn Camk2a/DTA mice treated with PBS (DC), MSCEVs (EV), and MSCGWEVs (GWEV), on exploring novel locations (panel E), exploring novel objects (panel F), and finding the platform in the water maze (panel G). Data are mean ± SEM (n = 8 mice in each group). *, $p \leq .05$; **, $p \leq .005$; ***, $p \leq .001$. Abbreviation: TRE, tetracycline/doxycycline response element.

hippocampi were isolated and subjected to Affymetrix Clariom D gene expression analysis. MSC-GWEV treatment of mice with hippocampal damage caused altered expression of more genes and changed expression levels to a greater extent of PBS treated mice with hippocampal damage than did treatment with MSC EVs (Fig. 4B). We subsequently emphasized comparisons of the genes altered by MSC GWEVs in the damaged hippocampus relative to the PBS treated controls. A total of 3,562 (5%) of the 65,614 analyzed mouse genes were differentially expressed (>twofold change) by hippocampi in MSC GWEV-injected Camk2a/DTA mice versus the PBS-injected mice. The genes with a twofold change were further analyzed using Partek GO enrichment analysis (Fig. 4C, 4D). The most significantly enriched functional group of the hippocampal genes differently expressed in MSC GWEV-injected versus PBS-injected Camk2a/DTA mice was in the "Immune system process" category; 18% of the differently expressed genes were involved in immune processes (Fig. 4C, 4D).

The 3,562 genes differentially expressed in MSC-GWEV versus PBS treated Camk2a/DTA mice were also subjected to Ingenuity Pathway Analysis (IPA) to explore the upstream regulators [60] of the MSC GWEV-affected genes in the damaged hippocampi (Fig. 4E). Among the top 14 major upstream regulators ($p < 3 \times 10^{-6}$), 11 regulators (INF-γ, TNF, CREM, TSC2, IL-10, CREB1, TGFβ, glucocorticoid receptor GR, IL-3, TGFβR2, IL-4) are involved in regulating inflammation (Fig. 4E, red bars). Supporting Information Figure S3 illustrates the relative expression of the genes which are controlled by these upstream regulators in the damaged hippocampi of MSC GWEV-treated Camk2a-DTA mice. The data also show that expression of genes involved in anti-inflammatory and BBB formation is elevated and the expression of genes involved in pro-inflammatory responses are suppressed (Supporting Information Fig. S3) in the damaged hippocampi of the GWEV-injected Camk2a/DTA mice. Both GO enrichment and IPA analyses suggest that EP$_4$ antagonist-elicited MSC EVs will attenuate inflammation-elicited hippocampal damage.

To explore the specific effects of EP$_4$ antagonist-elicited MSC GWEVs, in comparison with MSC EVs, on hippocampal damage we compared gene expression in the hippocampi of MSC EV-injected and MSC GWEV-injected Camk2a/DTA mice. Compared with the EV-conditioned hippocampus, the top 10 gene mRNAs elevated in the GWEV-conditioned hippocampus are Cdkn1a, Apold1, Cyr61, Mfsd2a, Zfp36, Nfkbia, Osmr, Fos, Dusp1, and C/EBPδ (Fig. 4F). These genes are involved in astrocyte differentiation (e.g., Cdkn1a), BBB formation (e.g., Cyr61, Apold1, Mfsd2a) [61], and anti-inflammatory responses (e.g., Zfp36, Nfkbia, Osmr, Dusp1, C/EBPδ), respectively.

Astrocyte proliferation, brain inflammation, and BBB leakage occurring in response to CNS damage are all associated with loss of CNS function [62–65]. Consequently, we next examined the effects of EP$_4$ antagonist-elicited MSC EVs on astrocyte differentiation, inflammation, and BBB formation in the damaged hippocampus, to determine which of these important properties might be modulated, like memory, learning, and cognition, by MSC GWEV treatment.

EP$_4$ Antagonist-Elicited MSC EVs Directly Suppress A1 Reactive Astrocyte Differentiation and Promote A2 Astrocyte Differentiation in Cell Culture

Astrocytes, the second most abundant cells in brain, modulate neuron survival and maintenance [66]. Astrocytes undergoing a transformation in brain injury and disease, a process called "reactive astrogliosis," become "reactive astrocytes." There are two types of reactive astrocytes, A1 "harmful" astrocytes and A2 "helpful" astrocytes [67]. A1 reactive astrocytes are characterized by the A1 marker complement component 3 (C3) and by increased levels, relative to nonreactive astrocytes and A2 astrocytes, of vimentin (Vim) and GFAP. A2 astrocytes express CD109 and COX-2 as A2 markers [68] and have, compared with A1 astrocytes, reduced GFAP levels. A1 astrocytes exert potent pro-inflammatory functions and are destructive to neurons and synapses. In contrast, A2 astrocytes upregulate many neurotrophic factors [67, 68]. A1 astrocytes are increased in response to CNS insults. Inhibition of A1 reactive astrogliosis after CNS damage prevents neuron death [68].

Cdkn1a is the gene with the highest expression difference between the EV-conditioned and GWEV-conditioned hippocampi (Fig. 4F). Cdkn1a is a cyclin-dependent kinase inhibitor that prevents terminal astrocytic differentiation [69, 70]. The induction of Cdkn1a expression in the GWEV-conditioned hippocampus suggested that EP$_4$ antagonist-elicited MSC EVs may affect astrocyte differentiation in response to hippocampal damage.

We first assessed the direct effect of EP$_4$ antagonist-elicited MSC EVs on astrocytic differentiation. Cultured hippocampal neural cells isolated from mouse hippocampi were subjected to astrocyte differentiation in cell culture. The induced astrocytes were then treated with PBS, MSC EVs, or MSC GWEVs. Compared with the PBS-treated astrocytes, the expressions of astrocyte markers GFAP, Vim, and CD44 were greatly induced in the MSC EV-treated astrocytes (Fig. 5A). Since the increased levels of GFAP and Vim are characteristics of A1 reactive astrocytes, the data suggest that MSC EVs promote differentiation into A1 astrocytes. In contrast, the MSC GWEV treatment prevented the increased expression of astrocyte markers GFAP and Vim in Camk2a/DTA mice. Instead, GWEV promoted the expression both of Cdkn1a, which prevents A1 terminal astrocytic differentiation, and of the A2 astrocyte markers CD109 (Fig. 5A) and COX-2 (Fig. 5B). These observations suggest that, while basal MSC EVs directly promote the formation of A1 reactive astrocytes, the EP$_4$ antagonist-elicited MSC EVs prevent differentiation into reactive A1 astrocytes, which can cause damage of brain neurons and synapses, and promote differentiation into A2 astrocytes, which are protective to the CNS.

EP$_4$ Antagonist-Elicited MSC EVs Suppress A1 Astrocytic Differentiation in the Damaged Hippocampus Early After Systemic Administration

We next investigated whether suppression of A1 astrocyte differentiation by EP$_4$ antagonist-elicited MSC EVs occurs in vivo in the damaged hippocampus. Two rounds of PBS, MSC EV or MSC GWEV injections were given to each Camk2a/DTA mouse after the 25-day Dox withdrawal. At 5 days and 30 days after the last injection, the mouse hippocampi were isolated and subjected to mRNA array analysis or to immunostaining analysis.

The hippocampi of Camk2a/DTA mice injected with MSC GWEVs expressed higher mRNA levels of A2 astrocyte markers (e.g., CD109, Emp1, Slc10a6, CD14 [68]) and lower levels of reactive A1 astrocyte markers (e.g., Ggta1, Psmb8, C3, C4a, C4b [68]) then did the hippocampi of Camk2a/DTA mice injected with MSC EVs. In addition, the expression of reactive A1 astrocyte inducers, including C1qa, C1qb, C1qc, C1ql1, and Cfh [68], was reduced in the hippocampi by GWEVs (Fig. 5C).
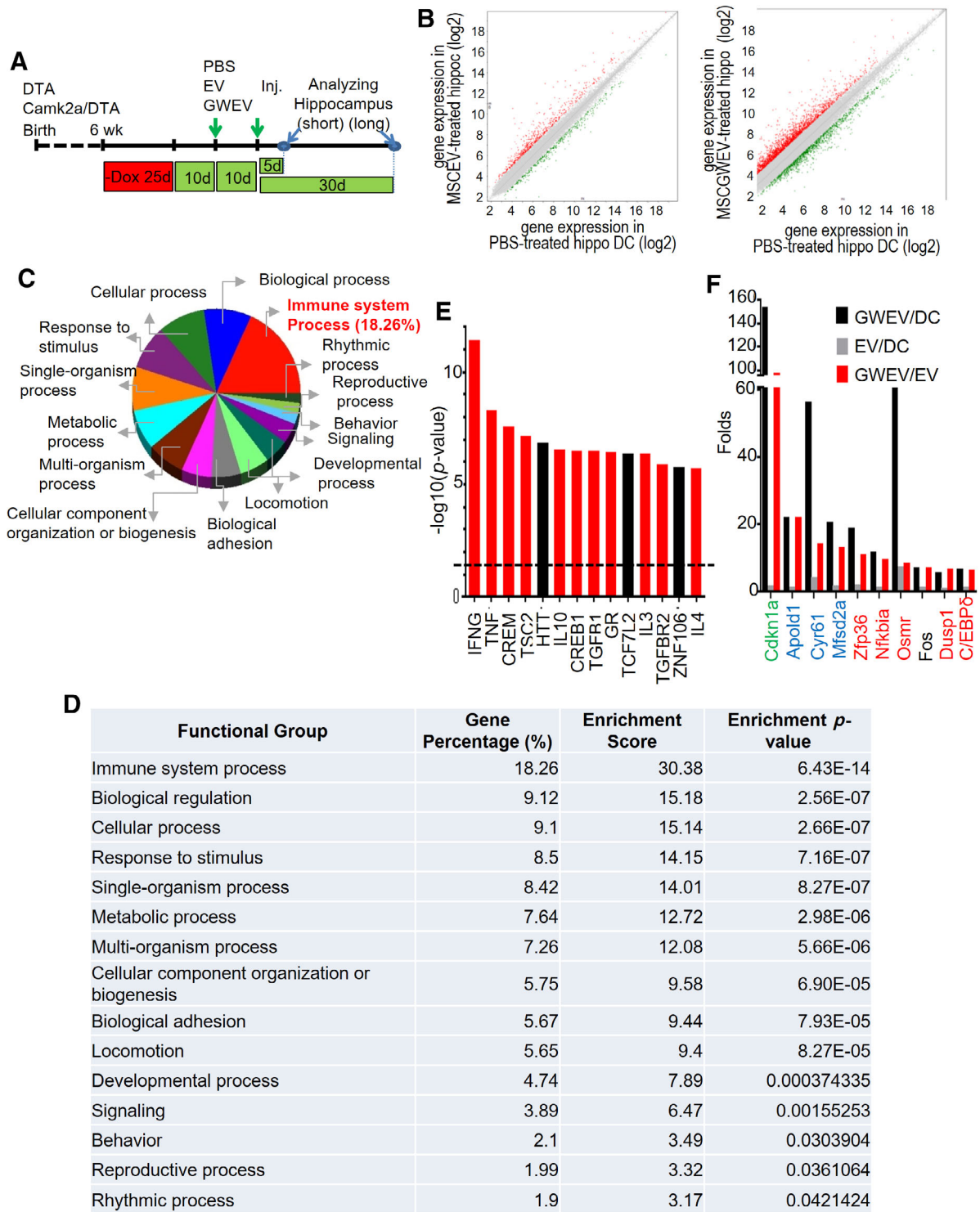
Figure 4. Prostaglandin E_2 receptor 4 (EP_4) antagonist-elicited mesenchymal stem cell (MSC) extracellular vesicles (EVs) increase the expression of genes involved in anti-inflammation in damaged hippocampus. **(A):** The scheme of the animal experiments, indicating the time points of damage induction, EV administration, and sample collection. **(B):** Levels of gene expression in the hippocampi of Dox-withdrawn Camk2a/DTA mice at 5 days after the treatment of phosphate-buffered saline (PBS), MSC EVs (MSCEV), or EP_4 antagonist-elicited MSC EVs (MSCGWEV). Red dots/green dots: genes with twofold higher/lower expression in EV-treated and GW-induced MSC EV (GWEV)-treated hippocampi. **(C, D):** Gene ontology enrichment analyses of the genes with greater than twofold different expression between PBS-treated and MSCGWEV-treated hippocampi. The pie chart shows the functional groups with an enrichment p-value <.05. The table shows gene percentage, enrichment score, and enrichment p-value of the functional groups. These values are calculated using Partek GO enrichment analysis. **(E):** Upstream regulators, identified using ingenuity pathway analysis, of the genes differentially expressed (>twofold) in PBS-treated and MSCGWEV-treated hippocampi. Red bars: regulators involved in anti-inflammation. **(F):** Top 10 mRNAs elevated in the MSC GWEV-conditioned hippocampi, compared with that of MSC EV-conditioned hippocampi. The bars indicate the fold expression of the genes for the mice treated as indicated in the panel.
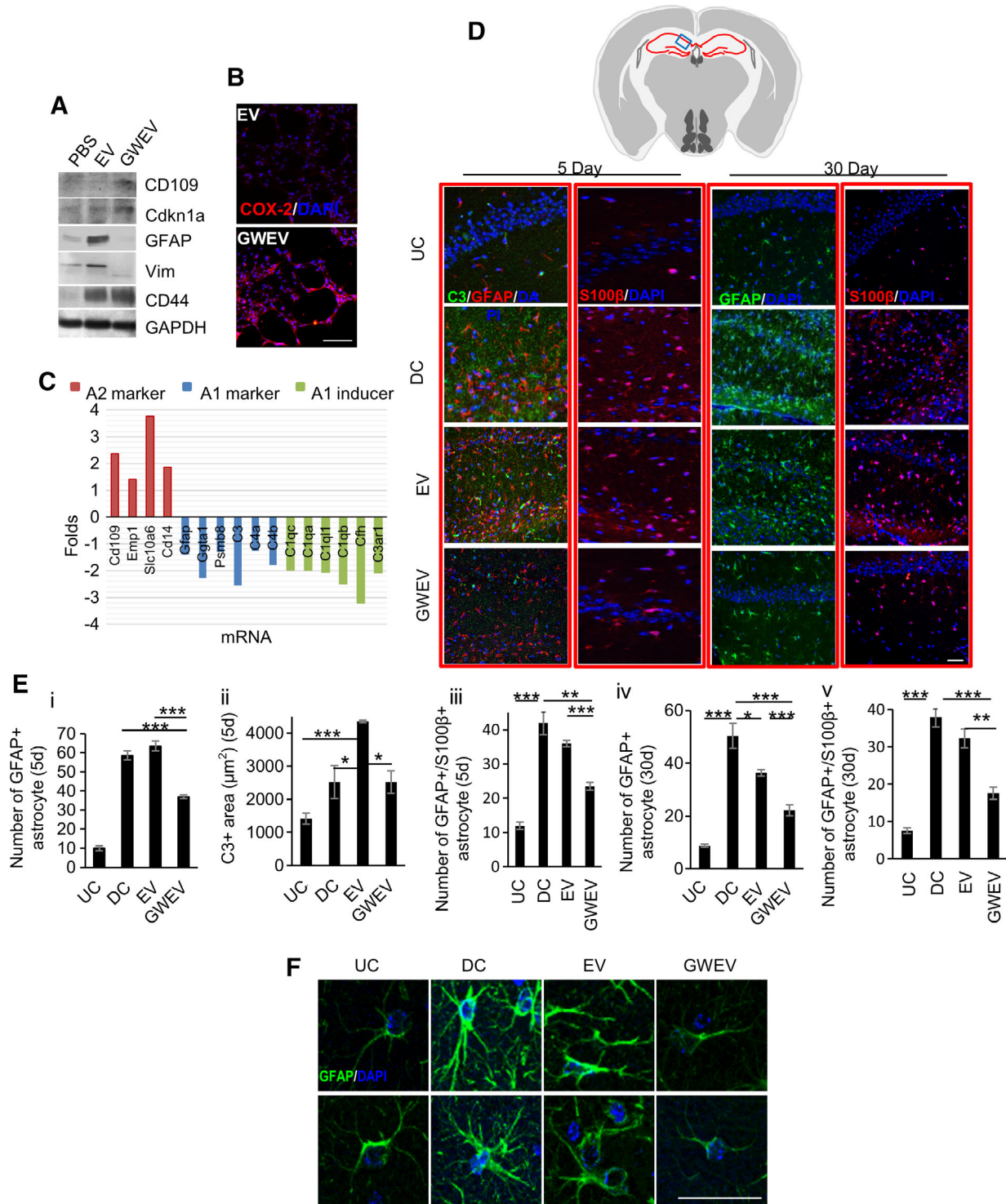
Figure 5. Prostaglandin E_2 receptor 4 antagonist-elicited mesenchymal stem cell (MSC) extracellular vesicles (EVs) suppress reactive astrogliosis. **(A):** Expression of A1 and A2 astrocyte markers was measured in phosphate-buffered saline (PBS)-treated, MSCEV-treated, and MSCGWEV-treated astrocytes. **(B):** Expression of A2 astrocyte marker COX-2 was analyzed in PBS-treated, MSCEV-treated, and MSCGWEV-treated astrocytes. Cell nuclei were stained with DAPI (blue). Scale bar: 50 μm. **(C):** Levels of astrocyte marker and inducer mRNA expression in the hippocampi of Dox-withdrawn Camk2a/DTA mice treated with MSCGWEVs, compared with that of the MSCEV-treated mice. **(D–F):** Immunofluorescence analyses of the hippocampi of Dox-withdrawn DTA mice (undamaged control) and Dox-withdrawn Camk2a/DTA mice at 5 days and 30 days after the treatment of PBS (damaged control), MSCEVs (EV), or MSCGWEVs (GWEV), using antibodies against C3, GFAP, and S100β. Cell nuclei were stained with DAPI (blue). Upper panel: the blue box in schematic depiction of the brain section represents the anatomic region analyzed by immunostaining. Red lines, hippocampus. Quantification of C3, GFAP⁺ astrocytes, and GFAP⁺/S100β⁺ astrocytes in hippocampi of mice is in panel (E). Data are mean ± SEM (n = 3 mice for each group). *, $p \leq .05$; **, $p \leq .005$; ***, $p \leq .001$. Images in panel (F) are 30-day hippocampal GFAP/DAPI images with higher magnifications from two mice in the indicated groups. Scale bar: 50 μm.

Compared with control DTA mice, there was a sixfold increase of GFAP$^+$ astrocytes in the hippocampal CA1 region of both PBS-injected and MSC EV-injected Camk2a/DTA mice (Fig. 5D, 5Ei). The increased A1 astrocyte marker C3 in MSC EV-injected CAamk2a/DTA mice suggested that systemic administration of MSC EVs increased appearance of destructive A1 reactive astrocytes in the damaged hippocampi (Fig. 5D, 5Eii). S100B in astrocytes alters synaptic plasticity and impairs spatial learning [71]. Increased S100B in astrocytes is associated with neural diseases such as CNS damage, amyotrophic lateral sclerosis, and AD [72, 73]. The destructive S100B-positive astrocytes increased in the damaged hippocampi of both PBS-injected and MSC EV-injected Camk2a/DTA mice, suggesting that MSC EVs cannot diminish astrogliosis-mediated damage (Fig. 5D, 5Eiii). In contrast, MSC GWEVs decreased the numbers of GFAP$^+$ astrocytes (Fig. 5D, 5Ei), the expression of A1 astrocyte marker C3 (Fig. 5D, 5Eii) and the number of S100B-positive astrocytes (Fig. 5D, 5Eiii) in the damaged hippocampi at the fifth day after systemic administration. These results suggest that EP$_4$-induced MSC GWEVs can suppress destructive astrogliosis in the damaged hippocampus shortly after administration, whereas MSC EVs have little or no suppressive effect on damage-induced astrogliosis.

The Suppression of Reactive Astrogliosis in the Damaged Hippocampus by EP$_4$ Antagonist-Elicited MSC EVs Is Sustained

At 30 days after PBS treatment we still observed increased levels of astrocytes in the PBS-injected Camk2a/DTA mice (Fig. 5D). Compared with DTA mice, there was still a fivefold increase of GFAP-positive astrocytes in the hippocampal CA1 region of PBS-injected Camk2a/DTA mice (Fig. 5Eiv). The astrocytes in PBS-injected Camk2a/DTA mice exhibited distinct morphological features of A1 reactive astrocytes; for example, thickened and increased astrocyte processes (Fig. 5F and Supporting Information Fig. S4). In contrast, the astrocytes in undamaged DTA mice presented only a few thin processes (Fig. 5F and Supporting Information Fig. S4). Compared with PBS-injected Camk2a/DTA mice, MSC EVs reduced the number of reactive astrocytes by only 26% in the damaged hippocampus CA1 at 30 days after their administration (Fig. 5D, 5Eiv). Moreover, the remaining astrocytes in the MSC EV-injected Camk2a/DTA mice maintained the morphological features of A1 reactive astrocytes (Fig. 5F and Supporting Information Fig. S4). In contrast, systemic MSC GWEV administration reduced by 60% the number of reactive astrocytes in the damaged CA1 hippocampi (Fig. 5D, 5Eiv) and the remaining astrocytes in the GWEV-injected Camk2a/DTA mice did not preserve the morphological features of A1 reactive astrocytes (Fig. 5F and Supporting Information Fig. S4). Although MSC GWEVs decreased by 60% destructive S100B-positive astrocytes, which can impair neuron functions in the damaged hippocampi, MSC EVs did not decrease S100B-positive astrocytes in the damaged hippocampus (Fig. 5D, 5Ev). In summary, EP$_4$ antagonist-elicited MSC GWEVs, in contrast to MSC EVs, reduce the presence of neurotoxic A1 reactive astrogliosis in the damaged hippocampus shortly after being delivered and the suppression is sustained and is increased subsequently.

EP$_4$ Antagonist-Elicited MSC EVs Decrease Microglia Infiltration in the Damaged Hippocampus

CNS inflammation is associated with an increase of microglia, the CNS resident immune cells that respond to pathogens and damaged cells. Microglia contribute to neuron death in brain damage

and neurodegenerative diseases [74]. EP$_4$ antagonist-elicited MSC GWEVs elicit anti-inflammatory genes in damaged hippocampi soon after their administration (Fig. 4), suggesting that the EP$_4$ antagonist-elicited MSC GWEVs may protect neurons by suppressing damage-induced hippocampal inflammation.

To measure the levels of microglia in hippocampal CA1, we analyzed the expression of the microglia marker Iba1 in the hippocampal CA1 of DTA mice and Camk2a/DTA mice injected with PBS, MSC EVs, or GWEVs at the fifth day after the injection. Only few Iba1-positive microglia were observed in undamaged hippocampi of the DTA mice. In contrast, the damaged Camk2a/DTA mice have massive microglia infiltration into the damaged CA1 regions (Fig. 6A). Although MSC EVs did not decrease the damaged-induced microglia infiltration into the damaged hippocampus early after the EV administration, MSC GWEVs decreased 40% of the damage induced-infiltration of microglia into the CA1 region at 5 days after EV administration (Fig. 6A).

Compared with undamaged mice, the massive microglia infiltration into the damaged CA1 regions were sustained in PBS-injected Camk2a/DTA mice at 30 days after the treatment of PBS (Fig. 6B). The induced CA1 damage caused a fivefold increase of microglia in the hippocampus (Fig. 6B). MSC EVs decreased 70% of the damaged induced microglia infiltration and MSC GWEVs decreased 90% of the infiltration at 30th day after administration (Fig. 6B). The effect of suppressing inflammation in the damaged hippocampus by EP$_4$ antagonist-elicited MSC GWEVs was observed early after administration and was enhanced subsequently.

EP$_4$ Antagonist-Elicited MSC EVs Restore the Integrity of the BBB in the Damaged Hippocampus

The role of the BBB is to maintain brain homeostasis, including the levels of various ions, neurotransmitters, and inflammatory cells in the brain [75]. The intact BBB reduces the traffic of inflammatory cells and minimizes inflammation of the damaged regions [75]. Thus, maintaining/restoring BBB integrity of a damaged brain is important to decrease brain inflammation and to restore brain neuron function.

Three (Apold1, Cyr61, Mfsd2a) of the 10 genes with the highest expression difference between MSC EV-conditioned and MSC GWEV-conditioned hippocampi are involved in BBB formation [61]; expression of these three BBB-associated genes was elevated in the damaged hippocampi of MSC GWEV-treated CamK2a/DTA mice (Fig. 4F). To examine BBB integrity in the damaged hippocampi in response to EV administration, expression of the BBB tight junction protein claudin-5 was measured in hippocampal extracts from mice at the fifth day after MSC EV injection (Fig. 6C). Loss of CLDN5 in tight junctions can increase BBB permeability and lead to neuronal cell death [76]. Increased CLDN5 expression is detected in stroke, as a compensatory mechanism to maintain tight junction and restore BBB function [77]. Compared with the MSC EV-injected Camk2a/DTA mice, the GWEV-injected Camk2a/DTA mice expressed increased hippocampal claudin-5 protein levels (Fig. 6C).

To further examine BBB tight junctions and their association with astrocytes under the sustained effects of MSC GWEVs, the hippocampi of Camk2a/DTA mice receiving PBS, MSC EV, or MSC GWEV injections were collected at the 30th day and analyzed for the expression and distribution of the tight junction protein claudin-5 and the astrocyte marker GFAP. Although organized claudin-5 expression was rarely observed around vasculatures in the damaged hippocampal CA1 of Camk2a/DTA injected with
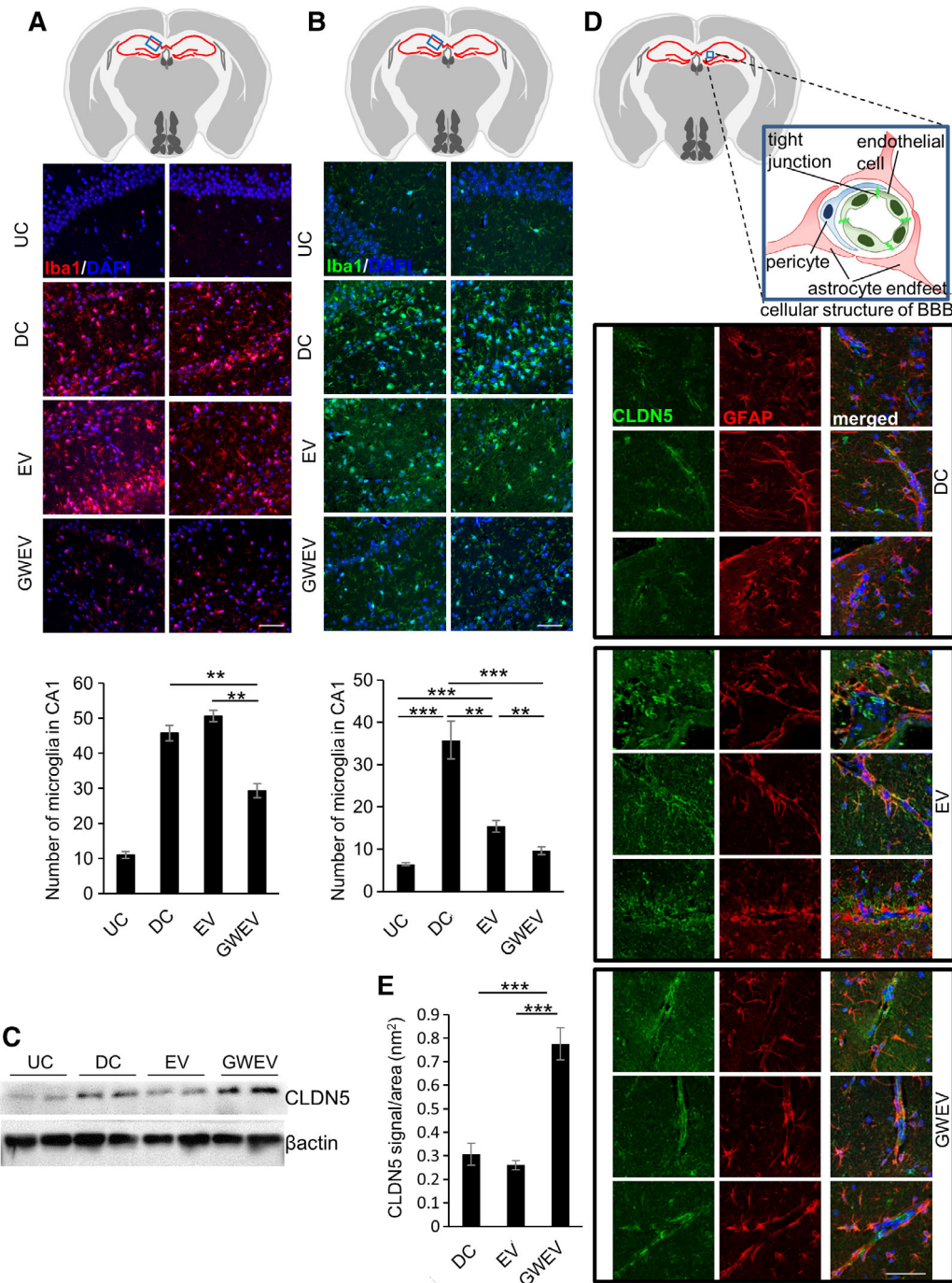
Figure 6. Prostaglandin E$_2$ receptor 4 antagonist-elicited mesenchymal stem cell (MSC) extracellular vesicles (EVs) suppress extensive inflammation and increase integrity of the blood–brain barrier (BBB) in damage hippocampi. **(A, B):** Immunofluorescence analyses for the hippocampi of Dox-withdrawn diphtheria toxin A (DTA) mice (undamaged control [UC]) and Dox-withdrawn Camk2a/DTA mice at 5 days (panel A) and 30 days (panel B) after treatment of PBS (damaged control [DC]), MSCEVs (EV), and MSCGWEVs (GWEV), using antibodies against the microglia marker Iba1. Upper panel: the blue box in schematic depiction of the brain section represents the anatomic region analyzed by immunostaining. Red lines, hippocampus. Cell nuclei were stained with DAPI (blue). Scale bar: 50 μm. The duplicate images are from the duplicate mice of each group. The bar charts show the numbers of Iba1$^+$ microglia in hippocampi of the mice as indicated. Data are mean ± SEM (n = 3 mice of each group). **, $p \leq .005$; ***, $p \leq .001$. **(C):** Levels of BBB tight junction protein claudin-5 (CLDN5) in the hippocampi of Dox-withdrawn DTA (UC) and Dox-withdrawn Camk2a/DTA mice treated with PBS (DC), MSCEVs, (EV), or MSCGWEVs (GWEV). **(D):** Immunofluorescence analyses for the hippocampi of Dox-withdrawn Camk2a/DTA mice at 5 days after treatment of PBS (DC), MSCEVs (EV), and MSCGWEVs (GWEV), using antibodies against CLDN5 and GFAP. Upper panel: the blue box in schematic depiction of the brain section represents the anatomic region, cellular structure of BBB, analyzed by immunostaining. Red lines, hippocampus. Cell nuclei were stained with DAPI (blue). Scale bar: 50 μm. The triplicate images are from three mice of each group. **(E):** Quantification of BBB tight junction protein CLDN5, normalized by area of perivascular GFAP-positive astrocyte endfeet which reflects size of the BBB structure, in hippocampi of the mice described in panel (D). Data are mean ± SEM (n = 8). ***, $p \leq .001$.

PBS or MSC EVs, the systemic administration of MSC GWEVs greatly increased claudin-5 protein present around cerebral vasculatures of Camk2a/DTA mice (Fig. 6D). In the MSC GWEV-injected Camk2a/DTA mice, the tight junction claudin-5 positive vasculature structures are located beside the GFAP positive-astrocyte endfeet (Fig. 6D). The levels of BBB tight junction claudin-5 were elevated in the MSC GWEV-injected Camk2a/DTA mice, but not in the MSC EV-injected Camk2a/DTA mice (Fig. 6E). These results suggest that EP_4 antagonist-elicited MSC GWEVs can elicit the repair of the damage-induced BBB disruption and restore the interaction between BBB and astrocytes to maintain CNS homeostasis.

In summary, we observed that EP_4 antagonist-elicited MSC EVs modulate the damaged hippocampal biological structure after systemic administration: (a) by reducing inflammatory responses, (b) by preventing A1 reactive astrogliosis (Fig. 5), (c) by blocking microglial infiltration into the damaged hippocampus (Fig. 6A, 6B), and (d) by maintaining BBB integrity (Fig. 6C, 6D). These effects are associated with restoring CNS functions [62–65], suggesting that the EP_4 antagonist-elicited MSC GWEV cellular effects described here may contribute to the MSC-GWEV rescue of memory and learning deficiencies caused by hippocampus damage.

DISCUSSION

MSCs have been used in preclinical and clinical studies to treat human diseases, including neurological diseases, by enhancing repair programs [78]. Several phase II and phase III studies of MSC-based therapies, including trials for neurological diseases, showed improvements compared with placebo [78]. However, the implanted MSCs do not achieve therapeutic effects by differentiating into the replacement tissues [79–81]. Many studies suggest paracrine signaling as the primary mechanism of MSC action [82, 83].

Our previous study demonstrated that blocking EP_4 signaling in mammary stem cells can induce the stem cells to release, via EVs, molecules which mediate stem cell properties [14]. Here, we report that EP_4 antagonism also increases EV release from MSCs and that the EP_4 antagonist-elicited MSC EVs, which are enriched in molecules essential for MSC properties, can fulfill the therapeutic potential suggested for MSCs. EP_4 antagonist-elicited MSC EVs (15 μg, two intracardiac injections) suppress astrogliosis and inflammation, and increase BBB integrity in damaged hippocampi. Finally, EP_4 antagonist-elicited MSC EVs can repair deficiencies of cognition, memory, and learning caused by damage in hippocampus CA1. In contrast, MSC EVs released in regular culture condition do not have these therapeutic effects.

MSCs are immune privileged; repeated administration of MSCs does not induce immunoreactivity or significant toxicity even to xenogeneic recipients [52–56]. The absence of immunoreactivity to MSCs allows the use of repeated MSC administration to potentiate the therapeutic effects of MSCs. It has been shown that the therapeutic effects are more pronounced in the repeated administrations of MSCs [84]. The lack of MSC immunogenicity allowed us to optimize the therapeutic effects of GW-treated MSC EVs by using two sequential injections.

MSCs can suppress the function of T cells and thus are tolerogenic [85, 86]. The immunosuppressive effects by MSCs appear to be mediated by MSC-released factors [87, 88]. A number of factors (i.e., IDO, iNOS, PGE2, TSG-6, and HLA-G) secreted by MSCs have been shown to mediate MSC immunoregulatory function. A number of studies report that MSCs EVs/exosomes exert MSC immunosuppressive functions by decreasing T and B cell proliferation and by inducing Treg cells [89–93]. Moreover, the immunomodulating factors are proposed to be packaged into EVs/exosomes [89]. Consequently, we gave repeated administrations of the MSC EVs/exosomes to mice with hippocampal damage, to potentiate the MSC therapeutic effects without toxicity caused by immunoreactivity. Like the work of others investigators [57], our results suggest that multiple administrations of xenogeneic MSC EVs/exosomes did not cause significant toxicity.

Figure 7 summarizes a model we postulate for the activity of EP_4-antagonist induced MSC EVs for many of the repair processes for damaged hippocampi. We observed that the neuronal DTA induced hippocampal damage is associated with reactive astrogliosis, extensive inflammation, broken BBB, and microglial infiltration into the damaged hippocampus (Fig. 7A). These phenotypes are consistent with pathologies of traumatic brain injury, stroke, and many neurodegenerative diseases (i.e., AD and PD) [63, 94, 95]. Damaged neurons are thought to induce reactive astrogliosis by releasing the inducer complement 1q (C1q) [96]. Increased neuroregeneration after brain trauma in $GFAP^{-/-}$ $Vim^{-/-}$ mice is reported to result from a decrease of reactive astrocytes [97]. This observation corresponds with our findings here that, in contrast to the basal MSC EVs, the EP_4 antagonist-elicited MSC EVs suppress reactive astrogliosis (Fig. 7B), presumably by directly suppressing the expression of GFAP and vimentin in astrocytes and by inhibiting the expression of reactive A1 astrocyte-inducer C1q.

Reactive astrogliosis is reported to cause both BBB disruption [98–100] and the production of factors (e.g., C3 and S100β) which activate microglia and impair neuron functions [71, 101] (Fig. 7A). The reactive astrocytes release C3, which then activates microglia. The activated microglia can also release C1q to promote reactive astrogliosis, which in turn exacerbates the activation of microglia and inflammation in a vicious cycle. The reduced expression of C1q and C3 in EP_4 antagonist-elicited MSC EVs treated hippocampi suggests that EP_4 antagonist-elicited MSC EVs disrupt this vicious activation cycle occurring among damaged neurons, reactive astrocytes, and microglia (Fig. 7B).

In contrast to basal MSC EVs, EP_4 antagonist-elicited EVs are enriched in anti-inflammation molecules (e.g., IL-2, IL-10, BDNF; Fig. 7B). Hippocampal gene expression analysis indicates that the genes most substantially differently expressed between basal MSC EV- and EP_4 antagonist-elicited EV-conditioned damaged hippocampi are primarily involved in immune processes and anti-inflammation. Five of the top 10 genes whose expression is increased in damaged hippocampi in response to EP_4 antagonist-elicited EVs have anti-inflammation activities (e.g., Zfp36 [102, 103], Nfkbia [104], Osmr [105, 106], Dusp1 [107, 108], C/EBPδ [109]). The anti-inflammatory effects of EP_4 antagonist-induced MSC EVs in damaged hippocampi are also reflected by decreasing microglia in damaged hippocampi. These data suggest that EP_4 antagonist-elicited MSC EVs can prevent brain dysfunction exacerbated by extensive inflammation in damaged hippocampi.

The BBB maintains brain homeostasis, in part by reducing entry of inflammatory cells (e.g., lymphocytes, neutrophils, and monocytes) into the brain [75]. The broken BBB cannot prevent entry of inflammatory cells into the damaged brain and, consequently,
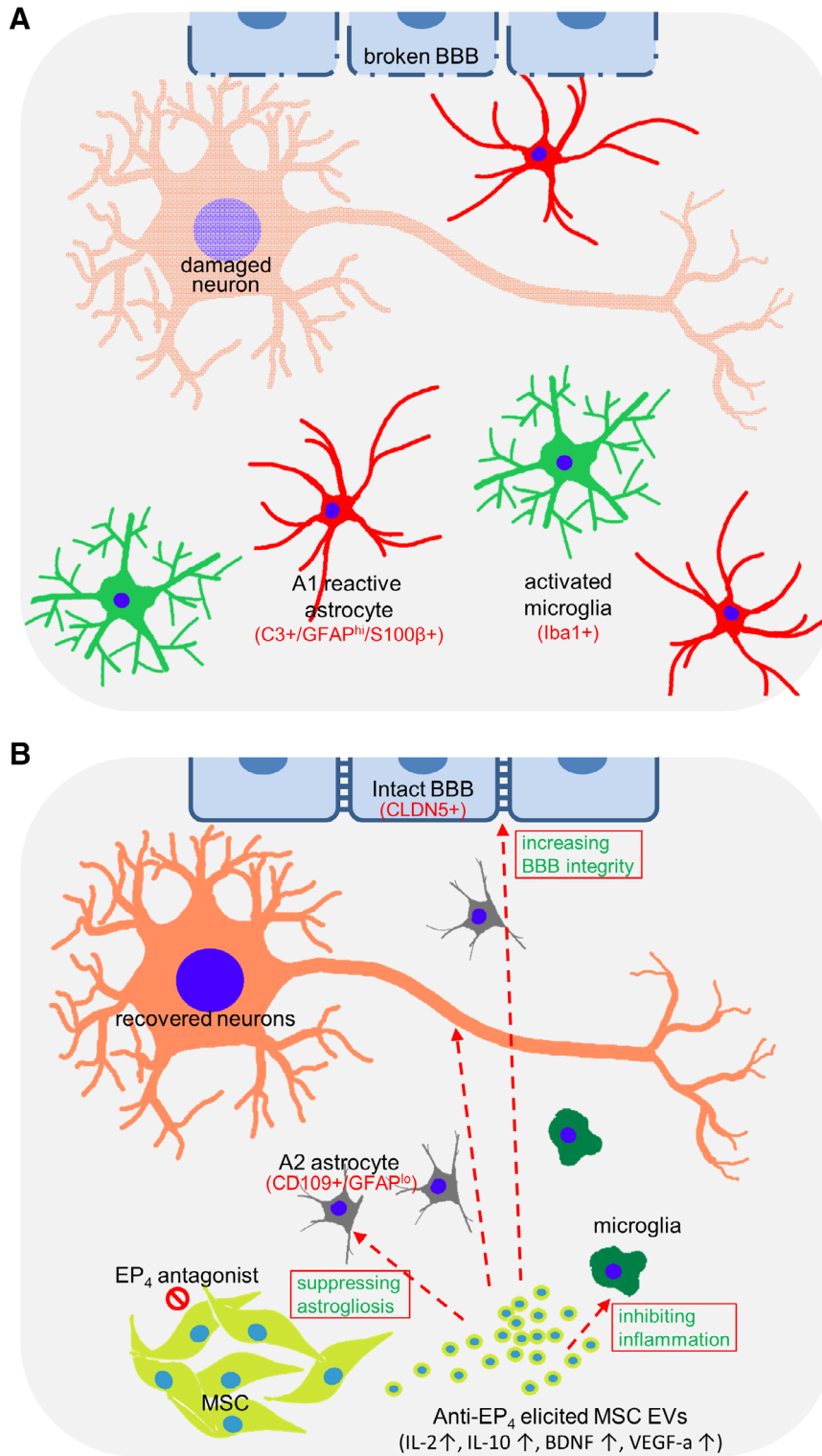
Figure 7. A proposed mechanism of CNS therapy by prostaglandin E₂ receptor 4 (EP₄) antagonist-elicited mesenchymal stem cell (MSC) extracellular vesicles. **(A, B):** The status of damaged hippocampi treated with phosphate-buffered saline (panel A) or EP₄ antagonist-elicited MSCEVs (panel B). **(A):** Hippocampal damage is associated with reactive astrogliosis, extensive inflammation, broken blood–brain barrier (BBB) and microglial infiltration into the damaged area. **(B):** EP₄ antagonist-elicited MSC EVs are enriched in IL-2, IL-10, VEGF-a, and BDNF. These and other cargo components of EP₄ antagonist-elicited MSC EVs suppress reactive astrogliosis and inflammation and allow the recovery of CNS neurons, the BBB and behavioral function.

cannot prevent an increase in inflammation of the damaged regions (Fig. 7A). On the other hand, BBB dysfunction can result in hypertrophy and GFAP and Vim upregulation in astrocytes, consequently triggering reactive astrogliosis [110]. Microglial activation induced by CNS damage can cause a loss of BBB integrity [111]. Thus, BBB disruption, reactive astrogliosis, extensive

inflammation and CNS damage drive each other in this amplifying circle, resulting in the loss of CNS function. In contrast to basal MSC EVs, EP_4 antagonist-elicited EVs are enriched in the BBB integrity-supporting factor TIMP1. Restoration of BBB integrity in damaged hippocampi by EP_4 antagonist-elicited MSC EVs is likely to contribute to the suppression of astrogliosis and inflammation, and to the functional recovery of the damaged hippocampi (Fig. 7B).

CONCLUSION

Here we demonstrate that blocking PGE_2/EP_4 signaling in MSCs promotes both targeted protein sorting into EVs and the subsequent increased release of EVs. We also demonstrate that EP_4 antagonist-elicited MSC EVs exhibit greatly enhanced therapeutic potential, in contrast to the comparatively low efficiency of EVs derived from untreated MSCs, to rescue several CNS pathologies; (e.g., reactive astrogliosis, extensive inflammation, disrupted BBB), which are often associated with brain injury, stroke and many neurodegenerative diseases (e.g., AD and PD). Our study suggests EP_4-antagonist elicited MSC EVs as a regenerative medicine for CNS diseases. We suggest that EP_4 antagonist-elicited MSC EVs may replace both MSCs [5, 6] and MSC EVs derived from untreated MSCs [57, 112, 113] in therapy for CNS disease and damage because both of increased therapeutic efficacy and of reduced adverse effects such as complications of implantation, ectopic tissue formation, and unwanted engraftment.

AUTHOR CONTRIBUTIONS

S.-Y.C.: conception and design, collection and/or assembly of data, data analysis and interpretation, manuscript writing; M.-C. L.: collection and/or assembly of data, data analysis and interpretation; J.-S.T.: collection of data, data analysis and interpretation; P.-L.H., W.-T.L.: collection of data; H.H.: conception and design, data analysis and interpretation, manuscript writing; H.-J.L.: conception and design, collection and/or assembly of data, data analysis and interpretation, manuscript writing, financial support, administrative support, final approval of manuscript.

DISCLOSURE OF POTENTIAL CONFLICTS OF INTEREST

The authors indicated no potential conflicts of interest.

DATA AVAILABILITY STATEMENT

The data that support the findings of this study are available from the corresponding author.

REFERENCES

1 Camicioli R, Moore MM, Kinney A et al. Parkinson's disease is associated with hippocampal atrophy. Mov Disord 2003;18: 784–790.

2 Braak H, Braak E. Neuropathological stageing of Alzheimer-related changes. Acta Neuropathol 1991;82:239–259.

3 Calabresi P, Castrioto A, Di Filippo M et al. New experimental and clinical links between the hippocampus and the dopaminergic system in Parkinson's disease. Lancet Neurol 2013;12: 811–821.

4 Pimentel-Coelho PM, Rosado-de-Castro PH, da Fonseca LM et al. Umbilical cord blood mononuclear cell transplantation for neonatal hypoxic-ischemic encephalopathy. Pediatr Res 2012;71:464–473.

5 van Velthoven CT, Sheldon RA, Kavelaars A et al. Mesenchymal stem cell transplantation attenuates brain injury after neonatal stroke. Stroke 2013;44:1426–1432.

6 Lunn JS, Sakowski SA, Hur J et al. Stem cell technology for neurodegenerative diseases. Ann Neurol 2011;70:353–361.

7 Chen A, Siow B, Blamire AM et al. Transplantation of magnetically labeled mesenchymal stem cells in a model of perinatal brain injury. Stem Cell Res 2010;5:255–266.

8 Marquez-Curtis LA, Janowska-Wieczorek A, McGann LE et al. Mesenchymal stromal cells derived from various tissues: Biological, clinical and cryopreservation aspects. Cryobiology 2015; 71:181–197.

9 Lee RH, Pulin AA, Seo MJ et al. Intravenous hMSCs improve myocardial infarction in mice because cells embolized in lung are activated to secrete the anti-inflammatory protein TSG-6. Cell Stem Cell 2009;5:54–63.

10 Zangi L, Margalit R, Reich-Zeliger S et al. Direct imaging of immune rejection and memory induction by allogeneic mesenchymal stromal cells. STEM CELLS 2009;27:2865–2874.

11 Caplan AI, Dennis JE. Mesenchymal stem cells as trophic mediators. J Cell Biochem 2006;98:1076–1084.

12 Thery C. Exosomes: Secreted vesicles and intercellular communications. F1000 Biol Rep 2011;3:15.

13 Marote A, Teixeira FG, Mendes-Pinheiro B et al. MSCs-derived exosomes: Cell-secreted nanovesicles with regenerative potential. Front Pharmacol 2016;7:231.

14 Lin MC, Chen SY, Tsai HM et al. PGE2/ EP4 signaling controls the transfer of the mammary stem cell state by lipid rafts in extracellular vesicles. STEM CELLS 2017;35:425–444.

15 Lin MC, Chen SY, He PL et al. PGE2/EP4 antagonism enhances tumor chemosensitivity by inducing extracellular vesicle-mediated clearance of cancer stem cells. Int J Cancer 2018;143: 1440–1455.

16 Lee BC, Kim HS, Shin TH et al. PGE2 maintains self-renewal of human adult stem cells via EP2-mediated autocrine signaling and its production is regulated by cell-to-cell contact. Sci Rep 2016;6:26298.

17 Kim HS, Shin TH, Lee BC et al. Human umbilical cord blood mesenchymal stem cells reduce colitis in mice by activating NOD2 signaling to COX2. Gastroenterology 2013;145: 1392–1403.

18 Chang JK, Li CJ, Wu SC et al. Effects of anti-inflammatory drugs on proliferation, cytotoxicity and osteogenesis in bone marrow mesenchymal stem cells. Biochem Pharmacol 2007;74:1371–1382.

19 Thery C, Amigorena S, Raposo G et al. Isolation and characterization of exosomes from cell culture supernatants and biological fluids. Curr Protoc Cell Biol 2006;30:3.22.1– 3.22.29

20 Mabuchi Y, Morikawa S, Harada S et al. LNGFR(+)THY-1(+)VCAM-1(hi+) cells reveal functionally distinct subpopulations in mesenchymal stem cells. Stem Cell Rep 2013;1:152–165.

21 Aslan H, Zilberman Y, Kandel L et al. Osteogenic differentiation of noncultured immunoisolated bone marrow-derived CD105+ cells. STEM CELLS 2006;24:1728–1737.

22 Yang YK, Ogando CR, Wang See C et al. Changes in phenotype and differentiation potential of human mesenchymal stem cells aging in vitro. Stem Cell Res Ther 2018; 9:131.

23 Gyorgy B, Szabo TG, Pasztoi M et al. Membrane vesicles, current state-of-the-art: Emerging role of extracellular vesicles. Cell Mol Life Sci 2011;68:2667–2688.

24 Olver C, Vidal M. Proteomic analysis of secreted exosomes. Subcell Biochem 2007; 43:99–131.

25 Hirabayashi Y, Itoh Y, Tabata H et al. The Wnt/beta-catenin pathway directs neuronal differentiation of cortical neural precursor cells. Development 2004;131:2791–2801.

26 Otero JJ, Fu W, Kan L et al. Beta-catenin signaling is required for neural

differentiation of embryonic stem cells. Development 2004;131:3545–3557.

27   Boregowda SV, Krishnappa V, Haga CL et al. A clinical indications prediction scale based on TWIST1 for human mesenchymal stem cells. EBioMedicine 2016;4:62–73.

28   Tsai CC, Chen YJ, Yew TL et al. Hypoxia inhibits senescence and maintains mesenchymal stem cell properties through downregulation of E2A-p21 by HIF-TWIST. Blood 2011;117:459–469.

29   Kyurkchiev D, Bochev I, Ivanova-Todorova E et al. Secretion of immunoregulatory cytokines by mesenchymal stem cells. World J Stem Cells 2014;6:552–570.

30   Banchereau J, Pascual V, O'Garra A. From IL-2 to IL-37: The expanding spectrum of anti-inflammatory cytokines. Nat Immunol 2012;13:925–931.

31   Rosenstein JM, Krum JM, Ruhrberg C. VEGF in the nervous system. Organogenesis 2010;6:107–114.

32   Oshima K, Teo DT, Senn P et al. LIF promotes neurogenesis and maintains neural precursors in cell populations derived from spiral ganglion stem cells. BMC Dev Biol 2007;7:112.

33   Segklia A, Seuntjens E, Elkouris M et al. Bmp7 regulates the survival, proliferation, and neurogenic properties of neural progenitor cells during corticogenesis in the mouse. PLoS One 2012;7:e34088.

34   Chen F, Radisky ES, Das P et al. TIMP-1 attenuates blood–brain barrier permeability in mice with acute liver failure. J Cereb Blood Flow Metab 2013;33:1041–1049.

35   Savarin C, Bergmann CC, Hinton DR et al. MMP-independent role of TIMP-1 at the blood–brain barrier during viral encephalomyelitis. ASN Neuro 2013;5:e00127.

36   Cheng A, Wang S, Cai J et al. Nitric oxide acts in a positive feedback loop with BDNF to regulate neural progenitor cell proliferation and differentiation in the mammalian brain. Dev Biol 2003;258:319–333.

37   Scharfman H, Goodman J, Macleod A et al. Increased neurogenesis and the ectopic granule cells after intrahippocampal BDNF infusion in adult rats. Exp Neurol 2005;192:348–356.

38   Xu D, Lian D, Wu J et al. Brain-derived neurotrophic factor reduces inflammation and hippocampal apoptosis in experimental *Streptococcus pneumoniae* meningitis. J Neuroinflammation 2017;14:156.

39   Tu Z, Li Y, Dai Y et al. MiR-140/BDNF axis regulates normal human astrocyte proliferation and LPS-induced IL-6 and TNF-alpha secretion. Biomed Pharmacother 2017;91:899–905.

40   Tripathy D, Thirumangalakudi L, Grammas P. RANTES upregulation in the Alzheimer's disease brain: A possible neuroprotective role. Neurobiol Aging 2010;31:8–16.

41   Sanchez A, Tripathy D, Grammas P. RANTES release contributes to the protective action of PACAP38 against sodium nitroprusside in cortical neurons. Neuropeptides 2009;43:315–320.

42   Courter LA, Shaffo FC, Ghogha A et al. BMP7-induced dendritic growth in sympathetic neurons requires p75(NTR) signaling. Dev Neurobiol 2016;76:1003–1013.

43   Yau SY, Li A, So KF. Involvement of adult hippocampal neurogenesis in learning and forgetting. Neural Plast 2015;2015:717958.

44   Cameron HA, Glover LR. Adult neurogenesis: Beyond learning and memory. Annu Rev Psychol 2015;66:53–81.

45   Hasan A, Deeb G, Rahal R et al. Mesenchymal stem cells in the treatment of traumatic brain injury. Front Neurol 2017;8:28.

46   Drago D, Cossetti C, Iraci N et al. The stem cell secretome and its role in brain repair. Biochimie 2013;95:2271–2285.

47   Mansilla E, Marin GH, Sturla F et al. Human mesenchymal stem cells are tolerized by mice and improve skin and spinal cord injuries. Transplant Proc 2005;37:292–294.

48   Mizuseki K, Diba K, Pastalkova E et al. Hippocampal CA1 pyramidal cells form functionally distinct sublayers. Nat Neurosci 2011;14:1174–1181.

49   Cerbai F, Lana D, Nosi D et al. The neuron-astrocyte-microglia triad in normal brain ageing and in a model of neuroinflammation in the rat hippocampus. PLoS One 2012;7:e45250.

50   Gusel'nikova VV, Korzhevskiy DE. NeuN as a neuronal nuclear antigen and neuron differentiation marker. Acta Nat 2015;7:42–47.

51   Clark RE, Broadbent NJ, Squire LR. Hippocampus and remote spatial memory in rats. Hippocampus 2005;15:260–272.

52   Saito T, Kuang JQ, Bittira B et al. Xenotransplant cardiac chimera: Immune tolerance of adult stem cells. Ann Thorac Surg 2002;74:19–24.

53   Wang Y, Han ZB, Ma J et al. A toxicity study of multiple-administration human umbilical cord mesenchymal stem cells in cynomolgus monkeys. Stem Cells Dev 2012;21:1401–1408.

54   Li J, Ezzelarab MB, Cooper DK. Do mesenchymal stem cells function across species barriers? Relevance for xenotransplantation. Xenotransplantation 2012;19:273–285.

55   Li J, Ezzelarab MB, Ayares D et al. The potential role of genetically-modified pig mesenchymal stromal cells in xenotransplantation. Stem Cell Rev 2014;10:79–85.

56   Grinnemo KH, Mansson A, Dellgren G et al. Xenoreactivity and engraftment of human mesenchymal stem cells transplanted into infarcted rat myocardium. J Thorac Cardiovasc Surg 2004;127:1293–1300.

57   Nakano M, Nagaishi K, Konari N et al. Bone marrow-derived mesenchymal stem cells improve diabetes-induced cognitive impairment by exosome transfer into damaged neurons and astrocytes. Sci Rep 2016;6:24805.

58   Mumby DG, Gaskin S, Glenn MJ et al. Hippocampal damage and exploratory preferences in rats: Memory for objects, places, and contexts. Learn Mem 2002;9:49–57.

59   Morris R. Developments of a water-maze procedure for studying spatial learning in the rat. J Neurosci Methods 1984;11:47–60.

60   Kramer A, Green J, Pollard J Jr et al. Causal analysis approaches in ingenuity pathway analysis. Bioinformatics 2014;30:523–530.

61   Hasan A, Pokeza N, Shaw L et al. The matricellular protein cysteine-rich protein 61 (CCN1/Cyr61) enhances physiological adaptation of retinal vessels and reduces pathological neovascularization associated with ischemic retinopathy. J Biol Chem 2011;286:9542–9554.

62   Pekny M, Pekna M. Astrocyte reactivity and reactive astrogliosis: Costs and benefits. Physiol Rev 2014;94:1077–1098.

63   Pekny M, Pekna M. Reactive gliosis in the pathogenesis of CNS diseases. Biochim Biophys Acta 1862;2016:483–491.

64   Erickson MA, Dohi K, Banks WA. Neuroinflammation: A common pathway in CNS diseases as mediated at the blood–brain barrier. Neuroimmunomodulation 2012;19:121–130.

65   Lucas SM, Rothwell NJ, Gibson RM. The role of inflammation in CNS injury and disease. Br J Pharmacol 2006;147:S232–S240.

66   Parpura V, Heneka MT, Montana V et al. Glial cells in (patho)physiology. J Neurochem 2012;121:4–27.

67   Liddelow SA, Barres BA. Reactive astrocytes: Production, function, and therapeutic potential. Immunity 2017;46:957–967.

68   Liddelow SA, Guttenplan KA, Clarke LE et al. Neurotoxic reactive astrocytes are induced by activated microglia. Nature 2017;541:481–487.

69   Kippin TE, Martens DJ, van der Kooy D. p21 loss compromises the relative quiescence of forebrain stem cell proliferation leading to exhaustion of their proliferation capacity. Genes Dev 2005;19:756–767.

70   Porlan E, Morante-Redolat JM, Marques-Torrejon MA et al. Transcriptional repression of Bmp2 by p21(Waf1/Cip1) links quiescence to neural stem cell maintenance. Nat Neurosci 2013;16:1567–1575.

71   Gerlai R, Wojtowicz JM, Marks A et al. Overexpression of a calcium-binding protein, S100 beta, in astrocytes alters synaptic plasticity and impairs spatial learning in transgenic mice. Learn Mem 1995;2:26–39.

72   Gonzalez-Martinez T, Perez-Pinera P, Diaz-Esnal B et al. S-100 proteins in the human peripheral nervous system. Microsc Res Tech 2003;60:633–638.

73   Donato R, Sorci G, Riuzzi F et al. S100B's double life: Intracellular regulator and extracellular signal. Biochim Biophys Acta 1793;2009:1008–1022.

74   Graeber MB, Li W, Rodriguez ML. Role of microglia in CNS inflammation. FEBS Lett 2011;585:3798–3805.

75   Varatharaj A, Galea I. The blood–brain barrier in systemic inflammation. Brain Behav Immun 2017;60:1–12.

76   Furuse M, Tsukita S. Claudins in occluding junctions of humans and flies. Trends Cell Biol 2006;16:181–188.

77   Du Y, Xu JT, Jin HN et al. Increased cerebral expressions of MMPs, CLDN5, OCLN, ZO1 and AQPs are associated with brain edema following fatal heat stroke. Sci Rep 2017;7:1691.

78   Squillaro T, Peluso G, Galderisi U. Clinical trials with mesenchymal stem cells: An update. Cell Transplant 2016;25:829–848.

79   Kunter U, Rong S, Boor P et al. Mesenchymal stem cells prevent progressive experimental renal failure but maldifferentiate into glomerular adipocytes. J Am Soc Nephrol 2007;18:1754–1764.

80   Aguilar S, Nye E, Chan J et al. Murine but not human mesenchymal stem cells generate osteosarcoma-like lesions in the lung. STEM CELLS 2007;25:1586–1594.

81   Fiorina P, Jurewicz M, Augello A et al. Immunomodulatory function of bone marrow-

derived mesenchymal stem cells in experimental autoimmune type 1 diabetes. J Immunol 2009;183:993–1004.

82 Phinney DG, Prockop DJ. Concise review: Mesenchymal stem/multipotent stromal cells: The state of transdifferentiation and modes of tissue repair—Current views. Stem Cells 2007;25:2896–2902.

83 van Poll D, Parekkadan B, Cho CH et al. Mesenchymal stem cell-derived molecules directly modulate hepatocellular death and regeneration in vitro and in vivo. Hepatology 2008;47:1634–1643.

84 Yang C, Wang G, Ma F et al. Repeated injections of human umbilical cord blood-derived mesenchymal stem cells significantly promotes functional recovery in rabbits with spinal cord injury of two noncontinuous segments. Stem Cell Res Ther 2018;9:136.

85 Ardanaz N, Vazquez FJ, Romero A et al. Inflammatory response to the administration of mesenchymal stem cells in an equine experimental model: Effect of autologous, and single and repeat doses of pooled allogeneic cells in healthy joints. BMC Vet Res 2016;12:65.

86 Poh KK, Sperry E, Young RG et al. Repeated direct endomyocardial transplantation of allogeneic mesenchymal stem cells: Safety of a high dose, "off-the-shelf", cellular cardiomyoplasty strategy. Int J Cardiol 2007;117:360–364.

87 Tse WT, Pendleton JD, Beyer WM et al. Suppression of allogeneic T-cell proliferation by human marrow stromal cells: Implications in transplantation. Transplantation 2003;75:389–397.

88 Di Nicola M, Carlo-Stella C, Magni M et al. Human bone marrow stromal cells suppress T-lymphocyte proliferation induced by cellular or nonspecific mitogenic stimuli. Blood 2002;99:3838–3843.

89 Cosenza S, Toupet K, Maumus M et al. Mesenchymal stem cells-derived exosomes are more immunosuppressive than microparticles in inflammatory arthritis. Theranostics 2018;8:1399–1410.

90 Del Fattore A, Luciano R, Pascucci L et al. Immunoregulatory effects of mesenchymal stem cell-derived extracellular vesicles on T lymphocytes. Cell Transplant 2015;24:2615–2627.

91 Blazquez R, Sanchez-Margallo FM, de la Rosa O et al. Immunomodulatory potential of human adipose mesenchymal stem cells derived exosomes on in vitro stimulated T cells. Front Immunol 2014;5:556.

92 Di Trapani M, Bassi G, Midolo M et al. Differential and transferable modulatory effects of mesenchymal stromal cell-derived extracellular vesicles on T, B, and NK cell functions. Sci Rep 2016;6:24120.

93 Monguio-Tortajada M, Roura S, Galvez-Monton C et al. Nanosized UCMSC-derived extracellular vesicles but not conditioned medium exclusively inhibit the inflammatory response of stimulated T cells: Implications for nanomedicine. Theranostics 2017;7:270–284.

94 Sofroniew MV, Vinters HV. Astrocytes: Biology and pathology. Acta Neuropathol 2010;119:7–35.

95 Takeda S, Sato N, Morishita R. Systemic inflammation, blood–brain barrier vulnerability and cognitive/non-cognitive symptoms in Alzheimer disease: Relevance to pathogenesis and therapy. Front Aging Neurosci 2014;6:171.

96 Stevens B, Allen NJ, Vazquez LE et al. The classical complement cascade mediates CNS synapse elimination. Cell 2007;131:1164–1178.

97 Wilhelmsson U, Li L, Pekna M et al. Absence of glial fibrillary acidic protein and vimentin prevents hypertrophy of astrocytic processes and improves post-traumatic regeneration. J Neurosci 2004;24:5016–5021.

98 Alvarez JI, Katayama T, Prat A. Glial influence on the blood–brain barrier. Glia 2013;61:1939–1958.

99 Cabezas R, Avila M, Gonzalez J et al. Astrocytic modulation of blood–brain barrier: Perspectives on Parkinson's disease. Front Cell Neurosci 2014;8:211.

100 Sofroniew MV. Molecular dissection of reactive astrogliosis and glial scar formation. Trends Neurosci 2009;32:638–647.

101 Lian H, Litvinchuk A, Chiang AC et al. Astrocyte-microglia cross talk through complement activation modulates amyloid pathology in mouse models of Alzheimer's disease. J Neurosci 2016;36:577–589.

102 Schaljo B, Kratochvill F, Gratz N et al. Tristetraprolin is required for full anti-inflammatory response of murine macrophages to IL-10. J Immunol 2009;183:1197–1206.

103 Patial S, Curtis AD 2nd, Lai WS et al. Enhanced stability of tristetraprolin mRNA protects mice against immune-mediated inflammatory pathologies. Proc Natl Acad Sci USA 2016;113:1865–1870.

104 Newton K, Dixit VM. Signaling in innate immunity and inflammation. Cold Spring Harb Perspect Biol 2012;4:a006049.

105 Hams E, Colmont CS, Dioszeghy V et al. Oncostatin M receptor-beta signaling limits monocytic cell recruitment in acute inflammation. J Immunol 2008;181:2174–2180.

106 Komori T, Tanaka M, Senba E et al. Lack of oncostatin M receptor beta leads to adipose tissue inflammation and insulin resistance by switching macrophage phenotype. J Biol Chem 2013;288:21861–21875.

107 Taylor DM, Moser R, Regulier E et al. MAP kinase phosphatase 1 (MKP-1/DUSP1) is neuroprotective in Huntington's disease via additive effects of JNK and p38 inhibition. J Neurosci 2013;33:2313–2325.

108 Liu Y, Shepherd EG, Nelin LD. MAPK phosphatases—Regulating the immune response. Nat Rev Immunol 2007;7:202–212.

109 Rustenhoven J, Scotter EL, Jansson D et al. An anti-inflammatory role for C/EBPdelta in human brain pericytes. Sci Rep 2015;5:12132.

110 O'Callaghan JP, Kelly KA, VanGilder RL et al. Early activation of STAT3 regulates reactive astrogliosis induced by diverse forms of neurotoxicity. PLoS One 2014;9:e102003.

111 Raj DD, Moser J, van der Pol SM et al. Enhanced microglial pro-inflammatory response to lipopolysaccharide correlates with brain infiltration and blood–brain barrier dysregulation in a mouse model of telomere shortening. Aging Cell 2015;14:1003–1013.

112 Xin H, Li Y, Cui Y et al. Systemic administration of exosomes released from mesenchymal stromal cells promote functional recovery and neurovascular plasticity after stroke in rats. J Cereb Blood Flow Metab 2013;33:1711–1715.

113 Zhang Y, Chopp M, Meng Y et al. Effect of exosomes derived from multipluripotent mesenchymal stromal cells on functional recovery and neurovascular plasticity in rats after traumatic brain injury. J Neurosurg 2015;122:856–867.

See www.StemCellsTM.com for supporting information available online.